NASA TM X-138

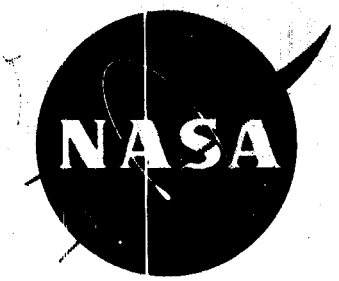

TECHNICAL MEMORANDUM

X-138

EFFECTS OF TWIST AND CAMBER AND THICKNESS ON THE AERODYNAMIC CHARACTERISTICS OF A 75° SWEPT ARROW WING AT A MACH NUMBER OF 2.91

By James N. Mueller and John E. Grimaud

Langley Research Center
Langley Field, Va.

Declassified December 8, 1961

NATIONAL AERONAUTICS AND SPACE ADMINISTRATION
WASHINGTON
December 1959

1N

NATIONAL AERONAUTICS AND SPACE ADMINISTRATION

TECHNICAL MEMORANDUM X-138

EFFECTS OF TWIST AND CAMBER AND THICKNESS ON THE AERODYNAMIC CHARACTERISTICS OF A 75° SWEPT ARROW WING AT A MACH NUMBER OF 2.91

By James N. Mueller and John E. Grimaud

SUMMARY

A wind-tunnel investigation has been made to evaluate the effects of twist and camber and thickness on the aerodynamic characteristics of a 75° swept arrow wing with an aspect ratio of 1.79 and a taper ratio of 0. Four wing-alone models were used in the investigation: two twisted and cambered wings of different thicknesses, and two nontwisted, noncambered wings ("flat" wings) with the same thickness and thickness distribution as the twisted and cambered wings. The tests were made at a Mach number of 2.91 and a Reynolds number of 1.5×10^6 with and without fixed transition.

The maximum lift-drag ratios $(L/D)_{max}$ of the twisted and cambered wings were less than those of the flat wings because of, in most part, the unfavorable drag characteristics of the former wings. The ratios of $(L/D)_{max}$ of the twisted and cambered wings to those of the flat wings were 0.91 and 0.96, respectively, for the thick- and thin-wing configurations. The effect of reducing the thickness of the twisted and cambered wing by about 28 percent was to increase $(L/D)_{max}$ by 12 percent, improve the trim characteristics, and to decrease the volume by 28 percent. The flat wings showed a 6-percent increase in $(L/D)_{max}$ with a decrease in thickness. Maximum lift-drag ratios measured on the twisted and cambered wings with fixed transition were 5.90 and 6.58, respectively, for the thick and thin wings. Measured $(L/D)_{max}$ of the twisted and cambered wings extrapolated to a Reynolds number of 10^8 produced values of 7.25 and 8.13 for the thick and thin wings, respectively. The relatively poor aerodynamic performance of the twisted and cambered wings as compared with that predicted by theory is attributed to the flow separation prevalent on the upper wing surfaces because of supercritical flow conditions. The wings were stable over the lift range of the tests, and the twisted and cambered wings exhibited excellent inherent trim characteristics.

INTRODUCTION

The Langley Research Center is participating in a program to provide basic information on the design of long-range bomber-type airplane configurations capable of cruise flight at Mach numbers near 3. Efficient cruise at a Mach number of 3 requires high lift-drag ratios. Certain aerodynamic approaches to attain a high lift-drag ratio which appear promising have been investigated both theoretically and experimentally. These approaches, as pointed out in reference 1, include development of favorable lift interference (refs. 2 to 8), the decrease of wave drag through thin component design (ref. 9), and the optimization of the total lift distribution for minimum induced drag (refs. 10 to 12). This paper is concerned with the latter approaches.

The concept of the twisted and cambered arrow wing is discussed in reference 13. This wing attempts to obtain a high lift-drag ratio by reducing the drag due to lift. The actual wing design is described in references 10 and 11. Some experimental results obtained on this wing have been reported in reference 14. The emphasis in reference 14 was on performing component tests of a complete configuration using this wing.

The present tests were conducted in the Langley 9-inch supersonic tunnel on wing-alone models, and were concerned with isolating and evaluating the effects of twist and camber and thickness on the aerodynamic characteristics of the twisted and cambered arrow wing. Results were obtained on the sting-mounted models at a Mach number of 2.91 and at a Reynolds number of 1.50×10^6 for both natural and fixed boundary-layer transition on the models.

SYMBOLS

The force- and moment-coefficient data are given with respect to the stability-axes system. The reference center for the moment data is at the apex of the wing trailing edge ($0.342\bar{c}$).

A	wing aspect ratio, b^2/S
b	wing span, ft
C_D	drag coefficient, $\frac{\text{Drag}}{qS}$
$C_{D,min}$	minimum drag coefficient
C_f	skin-friction coefficient

C_L	lift coefficient, $\frac{\text{Lift}}{qS}$
$C_{L,opt}$	lift coefficient at maximum L/D
C_{L_α}	lift-curve slope, per degree, at $C_L = 0$
C_m	pitching-moment coefficient, $\frac{\text{Pitching moment}}{qS\bar{c}}$
C_{m_α}	pitching-moment-curve slope per degree
$\bar{c}$	wing mean aerodynamic chord, ft
$\frac{dC_m}{dC_L}$	longitudinal static stability parameter
K	drag-due-to-lift parameter, $\frac{dC_D}{dC_L{}^2}$
L/D	lift-drag ratio
$(L/D)_{max}$	maximum lift-drag ratio
l	location of transition strip relative to wing leading edge (see fig. 1)
M	Mach number
p	static pressure, lb/sq ft
q	dynamic pressure, $\frac{\gamma}{2} M^2 p$, lb/sq ft
R	Reynolds number based on $\bar{c}$
S	wing area, sq ft
t/c	ratio of section thickness to section chord
w	width of transition strip (see fig. 1)
α	angle of attack, deg
γ	ratio of specific heats
ρ,σ,z	coordinate system for defining wing ordinates (see fig. 6)

Subscripts:

cr	critical
L	lower
U	upper

APPARATUS AND TESTS

Wind Tunnel, Balance, and Model Support

The investigation was conducted in the Langley 9-inch supersonic tunnel which is a continuous closed-return type of tunnel with provisions for the control of the humidity, temperature, and pressure of the enclosed air. During the tests the quantity of water vapor in the tunnel air was kept sufficiently low so that the effects of water condensation in the supersonic nozzle were negligible.

The balance system used in these tests was a six-component external type which utilized mechanical, self-balancing beams for the force measurements. A detailed description of this balance is presented in the appendix of reference 15.

The models were sting mounted to the model support of the external balance system (fig. 1). The model support and part of the sting were shielded from air loads by a movable windshield which was equipped with four pressure tubes open at the front of the windshield to measure the pressures on the rear of the sting shoulders. (These measured pressures are used to apply a correction to the drag data, as is explained in a later section.) The streamwise gap between the sting shoulder and the windshield snout was about 0.010 inch or less for all tests.

Models

Four wing-alone (wings mounted on low-drag stings), arrow-shaped plan-form models with leading-edge sweep of 75° were used in the present investigation. Two of the wings were twisted and cambered, differing only in thickness-chord ratio, and two wings were "flat" (no twist or camber) with the thickness-chord ratios corresponding to those for the twisted and cambered wings. Shown in figures 1 and 2 are drawings of the two types of wings used in this investigation. The thickness distributions of the wings are shown in figure 3. Figures 4 and 5 are photographs of the thick flat and thick twisted and cambered wing models, respectively. Table I, in conjunction with figure 6, which shows the

notations used in the table, gives the ordinates of the test wings. (Wing thickness I and wing thickness II, as shown in table I, refers to the thick and thin wings, respectively.) The square of wing thickness-chord ratio, measured at the wing-mean-aerodynamic-chord station, of the thick and thin wings are in the ratio of approximately 2 to 1.

The design of the twisted and cambered wings (ref. 13) utilizes linear theory. The plan form of the wings was selected on the basis of indications by the theory that rather large reductions in drag due to lift, as well as drag due to thickness, should be obtained by the use of sweptback wings with subsonic leading edges (ref. 16). The trailing-edge curvature was selected in an effort to reduce the magnitude of the pressure loading in the wing tip region (by an increase in local wing chords). The wings were cambered and twisted to provide a design lift coefficient of 0.1 at a Mach number of 3 by using the superposition method of references 10 and 11 and imposing the condition that the drag due to lift be a minimum for the plan form selected. A 63A thickness distribution, with the section normal to the leading edge, was then wrapped symmetrically around the mean camber surface. The overall thickness was determined approximately by the volume requirements for a long-range bomber design (exclusive of power plants). The wing alone was intended to be stable and to trim at the design point without the use of auxiliary longitudinal stabilizing surfaces; therefore, the concept for the complete airplane was that of the flying wing having little or no fuselage and with all required internal volume (exclusive of the power plant) provided by the wing.

All of the wings were mounted to low-drag-type stings of approximately the same dimensions. The small differences that do exist between the stings is due to fairing the stings into the wing surfaces at the forward part of the stings.

For ease of discussion, the nontwisted and noncambered wings will be referred to as the flat wings in the text to follow.

Tests

The tests were made at a Mach number of 2.91 and a Reynolds number of about 1.50×10^6, based on wing mean aerodynamic chord. All the wings were tested through an angle-of-attack range from -2° to 8° at zero sideslip angle. The tests were made with and without roughness strips (fixed transition) attached near the leading edges of the models. The roughness strips were composed of spherical aluminum oxide particles 0.005-0.008 inch in diameter affixed 3/32 inch rearward of the wing leading edge measured perpendicular to the leading edge. The transition strips were 1/16 inch wide.

Schlieren photographs of the wing models were obtained concurrently with the force tests, and some typical schlieren photographs are shown in figures 7 to 9.

Visualization of boundary-layer transition and flow-separation locations on the models were illustrated by liquid-film tests, similar to that described in references 17 and 18. Liquid-film photographs of the thick twisted and cambered wing are shown in figure 10.

Measurements, Corrections, and Accuracy

Lift, drag, and pitching moments of the models were measured on an external balance system. Angle of attack of the models was determined by an optical system. In this system, small (1/16-inch-diameter) mirrors are attached to the stings of the models. These mirrors reflect an image from an external light source onto a graduated scale.

Standard corrections for sting-mounted models in the Langley 9-inch tunnel were applied to the drag data of the configurations to account for the difference between free-stream static pressure and (1) the measured pressure on the base of the sting shoulders and (2) the pressure in the fixed-windshield—balance-box enclosure. This correction amounts to correcting the base of the sting to free-stream static-pressure conditions. The force coefficients do include the interference effects of, and forces on, the unshielded part of the sting, but this is known to be small (ref. 19).

The accuracy of the presented data based on balance calibration and repeatability is estimated to be within the following limits:

C_L	± 0.001
C_D	± 0.0002
C_m	± 0.002
L/D	± 0.15
M	± 0.01
α, deg	± 0.05
R	$\pm 0.02 \times 10^6$

RESULTS AND DISCUSSION

General

If full-scale flight conditions are to be predicted accurately from wind-tunnel model data, the state of the boundary layer (i.e., whether

laminar or turbulent) on the models must be known. It is convenient to have all turbulent flow over the test models when making extrapolations to full-scale conditions. Therefore, boundary-layer transition was fixed on the models by means of distributed granular-type roughness strips affixed to the wings near the leading edges. The appendix to this paper presents the results of a complementary test program to determine the size of transition strips to use on the test models in order to artifically promote boundary-layer transition. In addition, the wave drag due to the transition strip is assessed. This complementary test program showed that the transition-strip particle size used in the present tests definitely produced transition on the models, and that a small but not negligible wave drag due to the transition strips existed.

Basic Data

Figures 11 to 14 show the measured aerodynamic characteristics in pitch of the four wing models for the condition of natural and fixed boundary-layer transition.

The lift data for the flat wings (figs. 11 and 12) are generally linear with angle of attack throughout the angle-of-attack range of the tests. The lift data for the twisted and cambered wings (figs. 13 and 14) are seen to vary linearly with angle of attack up to about $C_L = 0.06$, at which point a gradual break to a lower lift-curve slope occurs. This loss in lifting efficiency is common for both the thick and thin wings with and without fixed transition. The reason for this lift loss is believed to be due to the existence of supercritical flow on the upper wing surface (the Mach number component in a direction normal to the wing leading edge becomes supersonic as the flow expands over the wing surface) and the fact that the resulting shock waves cause flow separation. The liquid-film photograph (fig. 10(a)) of the thick twisted and cambered wing indicates that separation does occur. (See refs. 17 and 18 for a more detailed discussion of the interpretation of liquid-film photographs.) The sharp demarkation between the dark and light areas roughly parallel to and slightly rearward of the leading edge on the right wing panel (fig. 10(a)) identifies the location at which the flow separates from the wing. The dark streaks (same panel) radiating from the apex are presumably flow disturbances such as vortices originating at the wing nose. Figure 7 of reference 14 which shows oil-film-flow photographs taken on a larger scale but similar wing, indicates essentially the same location of flow separation. Figure 10(a) further shows that although one wing panel is smooth and one wing panel has a fixed transition strip on it, the pattern of flow separation on the two wing panels is similar.

The bottom surface of the wing is shown in figure 10(b). The upper panel has a fixed transition strip attached near the leading edge, whereas

the lower panel is smooth. The panel with fixed transition appears to be drying faster, which indicates the presence of turbulent flow on this panel.

All of the wing models (figs. 11 to 14) exhibit a stable variation of pitching moment with angle of attack throughout the angle-of-attack range of the tests, and within the accuracy of the moment data the variations of C_m with α are linear.

Fixing boundary-layer transition on the models primarily affects the drag characteristics of the wings, as would be expected. It is seen (figs. 11 to 14) that the drag of the models is increased. This increase is attributed to the increase in skin friction due to increasing the extent of turbulent flow over the wings and to the wave drag caused by the roughness particles. A more detailed discussion concerning the technique and effects of fixing boundary-layer transition on the test models is contained in the appendix to this paper.

A summary of some of the aerodynamic parameters obtained on the wings of this investigation is given in table II.

Effects of Twist and Camber

Figure 15 shows the effects of twist and camber on the aerodynamic characteristics of the wing models for two thicknesses.

The lift-drag ratios for the twisted and cambered wings are less than those for the flat wings (figs. 15(a) and 15(b)). For the thick wings (fig. 15(a)), the maximum lift-drag ratio of the twisted and cambered wing is approximately $9\frac{1}{2}$ percent less than that of the flat wing. This lower lift-drag ratio of the twisted and cambered wing is due primarily to its unfavorable drag characteristics and, to a lesser extent, to the decrease in lifting effectiveness C_{L_α} for this wing relative to that for the flat wing at the higher values of C_L. (This can be seen by comparing fig. 11 with fig. 13.)

For the thin wings (fig. 15(b)), the maximum lift-drag ratios are more nearly the same (within 4 percent). The almost equal $(L/D)_{max}$ of these wings appears to be due principally to the favorable improvement in the drag characteristics of the twisted and cambered wing relative to that of the flat wing.

The minimum drags of the twisted and cambered wings are higher than those of the flat wings. This would be expected on the basis of design

considerations since the twisted and cambered wings depend primarily on their low drag-due-to-lift qualities to attain high lift-drag ratios.

The inherent good trim characteristics of the twisted and cambered wings as opposed to the unfavorable trim characteristics of the flat wings are shown in the plots of C_m against C_L (fig. 15). The thick twisted and cambered wing (fig. 15(a)) has a small positive pitching moment at $(L/D)_{max}$ which is favorable. The thin twisted and cambered wing is trimmed at $(L/D)_{max}$ (fig. 15(b)). In contrast, the thin flat wing indicates an out-of-trim diving moment at $(L/D)_{max}$. It is possible, then, that on the basis of trimmed flight conditions the thin twisted and cambered wing may have a greater value of $(L/D)_{max}$ than that of the thin flat wing.

Effects of Thickness

The effects of wing thickness on the aerodynamic characteristics of the flat and twisted and cambered wings are shown in figures 16(a) and 16(b), respectively. The relative wing thickness involved in these tests is such that $(t/c)^2$ (measured at the mean-aerodynamic-chord stations) is approximately 2 to 1.

Figure 16(a) shows that the effects of thickness on the aerodynamic characteristics of the flat wings are small. The maximum lift-drag ratio for the thin wing is about 6 percent greater than for the thick wing. Table II shows that the lift-curve slope of the thin wing is about 5 percent greater than for the thick wing. If it is assumed that the skin-friction drags for the two wings are equal, the decrease in $C_{D,min}$ with decrease in thickness is equivalent to that theoretically predicted by the variation of wave drag with $(t/c)^2$; that is, the wave drag of the thin wing is about one-half that of the thick wing.

The effects of thickness on the twisted and cambered wing (fig. 16(b)) are more pronounced than on the flat wings. The decrease in wing thickness produced an increase of 0.7 in the value of $(L/D)_{max}$ or about 12 percent. The increase in $(L/D)_{max}$ is due both to the drag reduction and to the increase in lift (6-percent increase in lift-curve slope) when the thickness was reduced. (See table II.) In addition to the decrease in drag from considerations of wing thickness alone, the drag characteristics probably improve due to an increase in the critical Mach number and a lessening of the transonic flow effects (shock-wave—boundary-layer interaction and attendant flow separation) on the upper wing surface.

It seems reasonable to assume that these effects exist on the thin wing although of less severity. In reference 13 it is shown that a 75° swept-back, zero thickness arrow wing at a lift coefficient of 0.1 has a free-stream $M_{cr} \approx 2.8$; whereas, for a wing with a 63A010 section normal to the leading edge at a lift coefficient of 0.1, $M_{cr} = 2.4$. The existence of supercritical flow over the upper surface of the wing is unfortunate because, as pointed out in reference 13 and as experimentally determined in reference 14, the drag due to lift becomes exceedingly large relative to the theoretically predicted value, and the penalty in wing aerodynamic efficiency is correspondingly large. Attaining subcritical flow over the wing sections at this Mach number, however, appears difficult to achieve at high sweep angles and large enough lift coefficients to be usable.

Reducing wing thickness is incompatible with airplane volume requirements. If it is assumed that wing volume is proportional to the wing thickness the penalty for an increase in $(L/D)_{max}$ of 0.7 is an estimated reduction in wing volume of approximately 28 percent. These results are in qualitative agreement with figure 9 of reference 12 which shows the variation of $(L/D)_{max}$ with the volume parameter $\frac{(\text{Volume})^{2/3}}{\text{Plan area}}$ of wings similar to the ones used in the present tests.

Effects of Fixed Transition on Lift-Drag Ratio

Figure 17 presents a summary of the results of lift-drag ratio for the four wings with and without transition in order to show the effects on $(L/D)_{max}$ of artificially producing turbulent flow over the test models. The reduction in $(L/D)_{max}$ of the models when the boundary-layer transition was fixed amounted to approximately 0.6, except for the thick twisted and cambered wing. For the thick twisted and cambered wing, however, the reduction in $(L/D)_{max}$ was only about one-half this value or about 0.3. This difference in the reduction in $(L/D)_{max}$, from that of the other wings, is possibly associated with loss in effectiveness of the upper surface transition strip due to flow separation.

Drag Due to Lift

Figure 18 shows the variation of C_D with C_L^2 of the test models, from which the drag-due-to-lift parameter $\left(dC_D/dC_L^2\right)$ is determined, and compares experiment with theory. The fixed-transition data are used in this figure in order that the true drags due to lift might not be masked by changes in the wing skin-friction drags due to changes in the percent

of laminar and turbulent flow over the models. The values of the drag-due-to-lift factors $K = \frac{dC_D}{dC_L^2}$ shown on the curves of figure 18 were obtained by evaluating the slopes of the curves at C_L^2 for $(L/D)_{max}$. This was done because the slopes of the curves for the twisted and cambered wings vary with C_L^2 as is characteristic of this type wing. For the flat wings, the curves are linear throughout most of the range of C_L^2. This method of evaluating the drag-due-to-lift factors for the twisted and cambered wings follows that employed in reference 1.

Figure 18 shows that the drag-due-to-lift values obtained experimentally do not approach closely the predicted values. These curves illustrate that the twisted and cambered wings, in particular, are failing to deliver the low drag due to lift for which they were specifically designed. For the thick twisted and cambered wing, the theoretical drag due to lift is about 45 percent less than that actually measured. Reducing the thickness-chord ratio of the wing did result in an experimental reduction in the K factor of about $9\frac{1}{2}$ percent (see fig. 18(b)), but this decrease in drag due to lift is relatively small when it is noted that the theoretical drag due to lift of the thin wing is still about 38 percent less than experiment.

The reason for the large discrepancy between predicted and experimental values of the drag-due-to-lift factors of the twisted and cambered wings is the large deviation of the actual upper-surface pressure distribution from those predicted by linear theory. It has been clearly established by experiment (ref. 14) that supercritical flow exists on the upper wing surfaces of the thick twisted and cambered wing and that transonic-flow effects, including shock-wave—boundary-layer interactions, and attendant flow separation are present. In addition, there is some question as to the applicability of linear theory at the Mach number of these tests, and its usefulness for the design of this type wing.

In reference 1, a complete airplane configuration using a twisted and cambered wing identical in design to the thick wing discussed previously, showed drag-due-to-lift values of about 0.7 at $M = 2.87$ and 0.5 at $M = 2.36$. This in itself indicates the powerful effects of Mach number on this performance parameter C_D/C_L^2 for this particular wing design.

Comparison of Theoretical and Experimental Results

The experimental data for the thick and thin twisted and cambered wings are compared with theoretical data, computed for $M = 3.00$, in figure 19. In general, the theoretical and experimental characteristics of the wings are in poor agreement for all comparisons made. The major contributing factor to the large disagreements between the predicted and measured wing characteristics is believed to be the aforementioned supercritical flow on the upper wing surface and the relatively high Mach number of these tests.

Full-Scale Extrapolation of $(L/D)_{max}$

In figure 20 the experimental values of $(L/D)_{max}$ obtained on the thick and thin twisted and cambered wings with transition fixed on the models are shown extrapolated to full-scale Reynolds numbers $\left(R = 10^8\right)$. The symbols in the lower center of the figure represent the experimental wind-tunnel values of $(L/D)_{max}$. The extrapolation of the experimental data is along the solid-line curves in the lower part of the figure. The dashed-line curves shown in the upper part of the figure show the extrapolated values of the theoretical wind-tunnel $(L/D)_{max}$ of the models. The extrapolations are based solely on the changes in skin-friction drag with Reynolds number; other effects are assumed equal.

The experimental extrapolated values of $(L/D)_{max}$ are considerably less than the predicted values for these wings. As shown, the estimated full-scale values of $(L/D)_{max}$ for the thick and thin wings are 8.13 and 7.25, respectively, as compared to predicted values of 11.25 and 9.91.

CONCLUSIONS

A wind-tunnel investigation has been made to evaluate the effects of twist and camber and thickness on the aerodynamic characteristics of a 75° swept arrow wing at a Mach number of 2.91 and a Reynolds number of 1.50×10^6 with and without fixed transition. An analysis of the results has led to the following conclusions:

1. The maximum lift-drag ratios $(L/D)_{max}$ of the twisted and cambered wings were less than those of the nontwisted, noncambered wings because of, in most part, the unfavorable drag characteristics of the former wings.

The ratios of $(L/D)_{max}$ of the twisted and cambered wings to those of the flat wings were 0.91 and 0.96, respectively, for the thick- and thin-wing configurations.

2. The effect of reducing the thickness of the twisted and cambered wing by about 28 percent was to increase $(L/D)_{max}$ by 12 percent, improve the trim characteristics, and to decrease the volume by 28 percent. The significant aerodynamic change due to thickness reduction for the flat wing was a 6-percent increase in $(L/D)_{max}$.

3. Maximum lift-drag ratios measured on the twisted and cambered wings with fixed transition were 5.90 and 6.58, respectively, for the thick and thin wings. Extrapolation of these values to a nominal full-scale Reynolds number of 10^8 produced values of 7.25 and 8.13, respectively, whereas corresponding theoretical estimates were 9.91 and 11.25.

4. The relatively poor aerodynamic performance of the twisted and cambered arrow wings as compared to theory is attributed to the flow separation prevalent on the upper wing surfaces, due to supercritical flow conditions. A contributing factor to the rather large disagreements between the theoretical and experimental results might be the questionable applicability of linear theory at the relatively high Mach number of these tests, and its usefulness for the design of this type wing.

5. The wings were longitudinally stable over the lift range of the tests, and the twisted and cambered wings exhibited excellent inherent trim characteristics.

Langley Research Center,
National Aeronautics and Space Administration,
Langley Field, Va., August 5, 1959.

APPENDIX

FIXED-TRANSITION STUDY

Several investigations (refs. 20 to 25) have been made at subsonic and supersonic speeds on the techniques of artificially producing turbulent boundary layers on models. These investigations - for example, references 21 and 25 - have sought, among other things, to determine the minimum particle size to use in the transition strip to assure a turbulent boundary layer over the model. Since this particle size is subject to individual tunnel characteristics and since no data existed at the time of these tests for Mach numbers as high as 3, a short test program was made to determine the grit size necessary to produce a turbulent boundary layer on the models.

The transition strips used on the wing models were of the distributed granular type and the particles themselves were pure aluminum oxide grains which are essentially spherical in shape. Three grain sizes (diameter) were used in the tests: 0.002-0.003 inch, 0.003-0.005 inch, and 0.005-0.008 inch. (These sizes correspond roughly to grit numbers of 320, 150, and 100, respectively.) The grains were applied to the models in the following steps:

(1) Clean model surface.
(2) Mask off area concerned with masking tape.
(3) Spray on adhesive smoothly with only one thin coat.
(4) Scatter on the aluminum oxide grains sparingly.
(5) Remove masking tape.
(6) Let strip air dry four hours or more.

As pointed out in reference 25, in order to minimize drag due to the particles they should be spread thinly in a narrow band.

In the tests on the models the measured $C_{D,min}$ of the models as compared to the estimated turbulent $C_{D,min}$ was relied on to indicate if all-turbulent flow was achieved on the models. Most of the grain-size tests were made on the flat wings (no twist, no camber). The Reynolds number range of the tests was from 0.78×10^6 to 2.80×10^6.

The results of this investigation are given in figures 21 and 22. In figure 21 the effects of grain size on minimum drag of the models are presented for several Reynolds numbers. Figures 21(a) and 21(b) are for the flat wings and figures 21(c) and 21(d) are for the twisted and cambered wings. The drag is plotted as a function of the square of the average grain-size diameter of the roughness particles used in the

transition strip. This follows supersonic wing theory practice in that the wave drag is proportional to the thickness squared. The analysis of the data follows that of unpublished data from the 8- by 7-foot supersonic test section of the Ames Unitary Plan wind tunnel, in which a similar limited fixed-transition study was made on several wing-body and complete configurations using different roughness grain sizes and at several Reynolds numbers.

In figures 21(a) and 21(b) a curve is faired, seemingly arbitrary, through the data. The fairing is partial to the data obtained at $R = 1.50 \times 10^6$. The reason for this is because the data presented in the main body of this paper were obtained at $R = 1.50 \times 10^6$. Also, from the Ames data plots it was found that the slope of the faired curve remained unchanged with Reynolds number, but varied from model to model. It was further stated that the latter effect would be expected as the quantity of grit on each model was not the same fraction of the wing area. In references 21 and 22, which are transition studies on bodies, it is noted that the curves of $C_{D,min}$ against grain size for a given Reynolds number reach a plateau once all-turbulent flow over the bodies is achieved, whereupon no increase in drag occurs with further increase in grain size. Of course, a drag increase would occur with further large increases in roughness height. For bodies, this type curve is characteristic, because the area of the roughness strip constitutes a small percentage of the body area; whereas, the ratio of the roughness strip frontal area on a wing to the wing frontal area would be expected to be much larger. Hence, the drag curve shows a continuous rise with increase in grain size. In figures 21(a) and 21(b) the intersection of the curves with the drag axis indicates the value of $C_{D,min}$ of the models for essentially all turbulent flows without roughness strips. The curve passes above the data point for the transition strips with grit 0.002-0.003 inch in diameter (fig. 21(a)), as this grit size failed to produce turbulent flow at the grit location. The drag values at point A (diamond symbol, figs. 21(a) and 21(b)) obtained for the models without roughness (smooth models) correspond to partially turbulent, partially laminar flow over the models. The $C_{D,min}$ increment B represents the drag increase resulting from producing essentially 100 percent turbulent flow over the models, whereas C is the wave drag increment for the transition strip with grit 0.005-0.008 inch in diameter. The increment C is measured from where the curve intersects the drag axis $\left(\text{for example, } C_{D,min} = 0.0073, \text{ fig. 21(a)}\right)$ to the data point obtained at $R = 1.50 \times 10^6$ for the roughness strips with grain 0.005-0.008 inch in diameter $\left(C_{D,min} = 0.0078\right)$. The 5-count increment shown by the data at $R = 1.50 \times 10^6$ in figure 21(b) appears reasonable when figure 21(a) is faired accordingly.

The data for the twisted and cambered wings (figs. 21(c) and 21(d)) are not faired. The fairings are omitted because of a lack of a sufficient number of data points, and also because the flow peculiarities on these wings can mask the true effects of the fixed transition strips. For example, flow separation known to exist on the upper wing surfaces of the thick wing could render the upper wing surface transition strip ineffective.

Two theoretical turbulent $C_{D,min}$ curves are shown in figure 22. The top curve (solid line) is based on skin-friction coefficients' values as given by Van Driest in reference 26, and the other turbulent curve is based on a skin-friction analysis using reference 27.

With reference to the flat-wing data shown in figure 22 it is seen that the smooth models are apparently in a transitional Reynolds number range, that is, the flow over the models is partly laminar and partly turbulent. When fixed transition strips are affixed to the models (square symbols) the drag is increased and falls slightly above the lower turbulent curve. Now if 5 counts of drag are deducted from these data points (the wave drag increment due to the fixed transition strips) the corrected data points fall within 3 counts of the lower turbulent drag curves. The same observation holds for the data point shown at $R = 2.80 \times 10^6$ for the thick flat wing; that is, if 5 counts are subtracted from the data point (triangular symbols) the corrected value is within about 3 counts of the lower turbulent curve.

Referring to figures 21(a) and 21(b) it is seen that the increment in drag (B) for all-turbulent flow over the thick and thin flat wings is about 9 and 12 counts, respectively. When these increments are added to the drag values obtained on the smooth models (fig. 22, circular symbols) the corrected drag values for these wings fall within 3 counts of the lower turbulent curve and roughly 9 counts below the Van Driest, or upper turbulent curve. It therefore appears that the curve based on Van Driest values of skin-friction coefficients may be slightly conservative.

The fixed transition data for the twisted and cambered wing showed several inconsistencies. It is believed that flow separation from the upper wing surfaces was the prime cause. For the thick wing (lower left plot, fig. 22) it is seen that at $R = 1.50 \times 10^6$ the effect of fixing transition on the model was to increase the drag about 4 counts or roughly equal to the wave drag of the wing roughness strip, as determined from the flat-wing data analysis. Increasing the Reynolds number to 2.80×10^6 (triangular symbol) placed the drag point between the two turbulent curves. If 5 counts are deducted from the drag value of this point the corrected data point would fall to within 1 drag count of the lower turbulent curve. The exact nature of the change in flow characteristics on the wing with increase in Reynolds number is not known quantitatively. However, flow

separation, prevalent at the lower Reynolds number, is reduced with increase in Reynolds numbers and the transition strips would be expected to become more effective.

The thin twisted and cambered wing drag data indicate similar changes with fixed transition and Reynolds number.

REFERENCES

1. Baals, Donald D., Toll, Thomas A., and Morris, Owen G.: Airplane Configurations for Cruise at a Mach Number of 3. NACA RM L58E14a, 1958.

2. Sleeman, William C., Jr.: Preliminary Study of Airplane Configurations Having Tail Surfaces Outboard of the Wing Tips. NACA RM L58B06, 1958.

3. Kelly, Thomas C., Carmel, Melvin M., and Gregory, Donald T.: An Exploratory Investigation at Mach Numbers of 2.50 and 2.87 of a Canard Bomber-Type Configuration Designed for Supersonic Cruise Flight. NACA RM L58B28, 1958.

4. Carmel, Melvin M., Kelly, Thomas C., and Gregory, Donald T.: Aerodynamic Characteristics at Mach Numbers From 2.5 to 3.5 of a Canard Bomber Configuration Designed for Supersonic Cruise Flight. NACA RM L58G16, 1958.

5. Church, James D., Hayes, William C., Jr., and Sleeman, William C., Jr.: Investigation of Aerodynamic Characteristics of an Airplane Configuration Having Tail Surfaces Outboard of the Wing Tips at Mach Numbers of 2.30, 2.97, and 3.51. NACA RM L58C25, 1958.

6. Dunning, Robert W.: Exploratory Investigation of the Longitudinal Aerodynamic Characteristics of a Canard Airplane Configuration at a Mach Number of 2.98. NASA MEMO 10-6-58L, 1958.

7. Rossow, Vernon J.: A Theoretical Study of the Lifting Efficiency at Supersonic Speeds of Wings Utilizing Indirect Lift Induced by Vertical Surfaces. NACA RM A55L08, 1956.

8. Ferri, Antonio, Clarke, Joseph H., and Cassacio, Anthony: Drag Reduction in Lifting Systems by Advantageous Use of Interference. PIBAL Rep. No. 272 (Contract No. AF 18(600)-694), Polytechnic Inst. Brooklyn, May 1955.

9. Mueller, James N., and Grimaud, John E.: A Wind-Tunnel Investigation To Evaluate the Aerodynamic Performance of Three Different Airplane Configurations Having Arrow- and Delta-Wing Plan Forms at a Mach Number of 2.91. NASA MEMO 3-11-59L, 1959.

10. Tucker, Warren A.: A Method for the Design of Sweptback Wings Warped To Produce Specified Flight Characteristics at Supersonic Speeds. NACA Rep. 1226, 1955. (Supersedes NACA RM L51F08.)

11. Grant, Frederick C.: The Proper Combination of Lift Loadings for Least Drag on a Supersonic Wing. NACA Rep. 1275, 1956. (Supersedes NACA TN 3533.)

12. Katzen, Elliott D.: Idealized Wings and Wing-Bodies at a Mach Number of 3. NACA TN 4361, 1958.

13. Brown, Clinton E., and McLean, Francis E.: The Problem of Obtaining High Lift-Drag Ratios at Supersonic Speeds. Jour. Aero/Space Sci., vol. 26, no. 5, May 1959, pp. 298-302.

14. Hallissy, Joseph M., Jr., and Hasson, Dennis F.: Aerodynamic Characteristics at Mach Numbers of 2.36 and 2.87 of an Airplane Configuration Having a Cambered Arrow Wing With a 75° Swept Leading Edge. NACA RM L58E21, 1958.

15. Rainey, Robert W.: Investigation of the Effects of Bomb-Bay Configuration Upon the Aerodynamic Characteristics of a Body With Circular Cross Sections at Supersonic Speeds. NACA RM L55E27, 1955.

16. Jones, Robert T., and Cohen, Doris: Aerodynamics of Wings at High Speeds. Aerodynamic Components of Aircraft at High Speeds. Vol. VII of High Speed Aerodynamic and Jet Propulsion, sec. A, A. F. Donovan and H. R. Lawrence, eds., Princeton Univ. Press, 1957, pp. 3-243.

17. Gray, W. E.: A Simple Visual Method for Recording Boundary Layer Transition (Liquid Film). Tech. Note No. Aero 1816, British R.A.E., Aug. 1946.

18. Vincenti, Walter G., Nielsen, Jack N., and Matteson, Frederick H.: Investigation of Wing Characteristics at a Mach Number of 1.53. I - Triangular Wings of Aspect Ratio 2. NACA RM A7I10, 1947.

19. Love, Eugene S.: Investigations at Supersonic Speeds of 22 Triangular Wings Representing Two Airfoil Sections for Each of 11 Apex Angles. NACA Rep. 1238, 1955. (Supersedes NACA RM L9D07.)

20. Winter, K. G., Scott-Wilson, J. B., and Davies, F. V.: Methods of Determination and of Fixing Boundary Layer Transition on Wind Tunnel Models at Supersonic Speeds. Tech. Note No. Aero.2341, British R.A.E., Sept. 1954.

21. Fallis, William B.: On Distributed Roughness as a Means of Fixing Transition at High Supersonic Speeds. Jour. Aero. Sci. (Readers' Forum), vol. 22, no. 5, May 1955, p. 339.

22. Luther, Marvin: Fixing Boundary-Layer Transition on Supersonic-Wind-Tunnel Models (II). Progress Rep. No. 20-287 (Contract No. DA-04-495-Ord 18), Jet Propulsion Lab., C.I.T., Feb. 1, 1956.

23. Von Doenhoff, Albert E., and Horton, Elmer A.: A Low-Speed Experimental Investigation of the Effect of a Sandpaper Type of Roughness on Boundary-Layer Transition. NACA Rep. 1349, 1958. (Supersedes NACA TN 3858.)

24. Braslow, Albert L.: Effect of Distributed Granular-Type Roughness on Boundary-Layer Transition at Supersonic Speeds With and Without Surface Cooling. NACA RM L58A17, 1958.

25. Braslow, Albert L., and Knox, Eugene C.: Simplified Method for Determination of Critical Height of Distributed Roughness Particles for Boundary-Layer Transition at Mach Numbers From 0 to 5. NACA TN 4363, 1958.

26. Van Driest, E. R.: Turbulent Boundary Layer in Compressible Fluids. Jour. Aero. Sci., vol. 18, no. 3, Mar. 1951, pp. 145-160, 216.

27. Sommer, Simon C., and Short, Barbara J.: Free-Flight Measurements of Turbulent-Boundary-Layer Skin Friction in the Presence of Severe Aerodynamic Heating at Mach Numbers From 2.8 to 7.0. NACA TN 3391, 1955.

TABLE I.- WING ORDINATES

(a) Flat wing, wing thickness I (thick)

$\frac{\rho}{b/2}$	$\frac{\sigma}{b/2}$	$\frac{z_U}{b/2}$	$\frac{z_L}{b/2}$
0	0	0	0
0.2	0	0	0
	.0010	.0032	-.0032
	.0030	.0048	-.0048
	.0050	.0062	-.0062
	.0101	.0085	-.0085
	.0153	.0105	-.0105
	.0205	.0121	-.0121
	.0259	.0135	-.0135
	.0313	.0148	-.0148
	.0367	.0161	-.0161
	.0423	.0172	-.0172
	.0479	.0183	-.0183
	.0536	.0195	-.0195
0.4	0	0	0
	.0020	.0042	-.0042
	.0040	.0060	-.0060
	.0080	.0079	-.0079
	.0101	.0090	-.0090
	.0113	.0113	-.0113
	.0203		
	.0254	.0142	-.0142
	.0358	.0167	-.0167
	.0411	.0179	-.0179
	.0464	.0190	-.0190
	.0517	.0201	-.0201
	.0571	.0210	-.0210
	.0625	.0218	-.0218
	.0679	.0227	-.0227
	.0735	.0235	-.0235
	.0790	.0243	-.0243
	.0845	.0249	-.0249
	.0901	.0256	-.0256
	.0958	.0262	-.0262
	.1015	.0268	-.0268
	.1072	.0274	-.0274

$\frac{\rho}{b/2}$	$\frac{\sigma}{b/2}$	$\frac{z_U}{b/2}$	$\frac{z_L}{b/2}$
0.6	0	0	0
	.0030	.0055	-.0055
	.0060	.0069	-.0069
	.0090	.0085	-.0085
	.0121	.0101	-.0101
	.0151	.0114	-.0114
	.0227	.0137	-.0137
	.0304	.0160	-.0160
	.0381	.0177	-.0177
	.0459	.0195	-.0195
	.0538	.0209	-.0209
	.0616	.0223	-.0223
	.0696	.0234	-.0234
	.0776	.0247	-.0247
	.0857	.0257	-.0257
	.0938	.0265	-.0265
	.1019	.0274	-.0274
	.1102	.0283	-.0283
	.1184	.0290	-.0290
	.1268	.0296	-.0296
	.1352	.0303	-.0303
	.1437	.0308	-.0308
	.1522	.0313	-.0313
	.1608	.0318	-.0318
0.8	0	0	0
	.0040	.0059	-.0059
	.0080	.0079	-.0079
	.0120	.0101	-.0101
	.0161	.0117	-.0117
	.0201	.0128	-.0128
	.0303	.0159	-.0159
	.0406	.0182	-.0182
	.0509	.0204	-.0204
	.0612	.0221	-.0221
	.0717	.0238	-.0238
	.0822	.0251	-.0251
	.0928	.0264	-.0264
	.1034	.0276	-.0276
	.1142	.0285	-.0285
	.1250	.0294	-.0294
	.1359	.0302	-.0302
	.1469	.0308	-.0308
	.1579	.0314	-.0314
	.1690	.0319	-.0319
	.1803	.0323	-.0323
	.1916	.0325	-.0325
	.2029	.0327	-.0327
	.2144	.0327	-.0327

TABLE I.- WING ORDINATES - Continued

(a) Flat wing, wing thickness I (thick) - Continued

$\frac{\rho}{b/2}$	$\frac{\sigma}{b/2}$	$\frac{z_U}{b/2}$	$\frac{z_L}{b/2}$
1.0	0	0	0
	.0050	.0063	-.0063
	.0100	.0089	-.0089
	.0151	.0110	-.0110
	.0201	.0126	-.0126
	.0252	.0139	-.0139
	.0379	.0172	-.0172
	.0507	.0197	-.0197
	.0635	.0219	-.0219
	.0765	.0237	-.0237
	.0896	.0252	-.0252
	.1027	.0266	-.0266
	.1160	.0278	-.0278
	.1293	.0287	-.0287
	.1428	.0295	-.0295
	.1563	.0302	-.0302
	.1699	.0307	-.0307
	.1836	.0310	-.0310
	.1974	.0312	-.0312
	.2113	.0313	-.0313
	.2253	.0311	- 0311
	.2394	.0307	-.0307
	.2536	.0303	-.0303
	.2679	.0260	-.0260
1.2	0	0	0
	.0060	.0065	-.0065
	.0120	.0095	-.0095
	.0181	.0115	-.0115
	.0241	.0131	-.0131
	.0302	.0149	-.0149
	.0455	.0182	-.0182
	.0608	.0207	-.0207
	.0763	.0227	-.0227
	.0919	.0245	-.0245
	.1075	.0260	-.0260
	.1233	.0271	-.0271
	.1392	.0281	-.0281
	.1552	.0288	-.0288
	.1713	.0293	-.0293
	.1875	.0296	-.0296
	.2039	.0296	-.0296
	.2203	.0294	-.0294
	.2369	.0289	-.0289
	.2536	.0283	-.0283
	.2704	.0274	-.0274
	.2873	.0264	-.0264
	.3044	.0252	-.0252
	.3215	.0238	-.0238

$\frac{\rho}{b/2}$	$\frac{\sigma}{b/2}$	$\frac{z_U}{b/2}$	$\frac{z_L}{b/2}$
1.4	0	0	0
	.0070	.0069	-.0069
	.0140	.0102	-.0102
	.0211	.0122	-.0122
	.0282	.0141	-.0141
	.0352	.0158	-.0158
	.0530	.0192	-.0192
	.0710	.0217	-.0217
	.0890	.0237	-.0237
	.1071	.0254	-.0254
	.1254	.0267	-.0267
	.1439	.0276	-.0276
	.1624	.0283	-.0283
	.1811	.0286	-.0286
	.1999	.0286	-.0286
	.2188	.0283	-.0283
	.2378	.0276	-.0276
	.2571	.0267	-.0267
	.2764	.0255	-.0255
	.2959	.0238	-.0238
	.3155	.0225	-.0225
	.3352	.0207	-.0207
	.3551	.0187	-.0187
	.3751	.0166	-.0166
1.6	0	0	0
	.0080	.0079	-.0079
	.0160	.0104	-.0104
	.0241	.0133	-.0133
	.0322	.0153	-.0153
	.0403	.0173	-.0173
	.0606	.0206	-.0206
	.0811	.0233	-.0233
	.1017	.0253	-.0253
	.1225	.0268	-.0268
	.1433	.0279	-.0279
	.1644	.0285	-.0285
	.1856	.0287	-.0287
	.2069	.0284	-.0284
	.2284	.0276	-.0276
	.2501	.0266	-.0266
	.2718	.0251	-.0251
	.2938	.0234	-.0234
	.3159	.0213	-.0213
	.3381	.0190	-.0190
	.3605	.0165	-.0165
	.3831	.0140	-.0140
	.4058	.0114	-.0114
	.4287	.0088	-.0088

TABLE I.- WING ORDINATES - Continued

(a) Flat wing, wing thickness I (thick) - Continued

$\frac{\rho}{b/2}$	$\frac{\sigma}{b/2}$	$\frac{z_U}{b/2}$	$\frac{z_L}{b/2}$
1.8	0	0	0
	.0011	.0085	-.0085
	.0180	.0122	-.0122
	.0271	.0149	-.0149
	.0362	.0172	-.0172
	.0453	.0190	-.0190
	.0682	.0228	- 0228
	.0912	.0254	-.0254
	.1144	.0274	-.0274
	.1378	.0287	-.0287
	.1613	.0294	-.0294
	.1850	.0295	-.0295
	.2088	.0289	-.0289
	.2328	.0277	-.0277
	.2570	.0262	-.0262
	.2813	.0241	-.0241
	.3058	.0217	-.0217
	.3305	.0189	-.0189
	.3554	.0158	-.0158
	.3804	.0128	-.0128
	.4056	.0097	-.0097
	.4310	.0064	-.0064
	.4565	.0035	-.0035
	.4823	.0003	-.0003
2.0	0	0	0
	.0100	.0097	-.0097
	.0201	.0134	-.0134
	.0301	.0165	-.0165
	.0402	.0190	-.0190
	.0503	.0208	-.0208
	.0758	.0247	-.0247
	.1014	.0275	-.0275
	.1271	.0293	-.0293
	.1531	.0302	-.0302
	.1792	.0302	-.0302
	.2055	.0294	-.0294
	.2320	.0279	-.0279
	.2587	.0257	-.0257
	.2855	.0230	-.0230
	.3126	.0198	-.0198
	.3398	.0162	-.0162
	.3672	.0127	-.0127
	.3948	.0090	-.0090
	.4226	.0053	-.0053
	.4507	.0016	-.0016
	.4620	.0001	-.0001

$\frac{\rho}{b/2}$	$\frac{\sigma}{b/2}$	$\frac{z_U}{b/2}$	$\frac{z_L}{b/2}$
2.2	0	0	0
	.0010	.0104	-.0104
	.0221	.0144	-.0144
	.0331	.0175	-.0175
	.0442	.0200	-.0200
	.0554	.0221	-.0221
	.0833	.0258	-.0258
	.1115	.0283	-.0283
	.1398	.0297	-.0297
	.1684	.0299	-.0299
	.1971	.0290	-.0290
	.2261	.0272	-.0272
	.2552	.0246	-.0246
	.2845	.0212	-.0212
	.3141	.0174	-.0174
	.3438	.0133	-.0133
	.3738	.0092	-.0092
	.4039	.0051	-.0051
	.4343	.0008	-.0008
	.4401	.0001	-.0001
2.4	0	0	0
	.0120	.0114	-.0114
	.0241	.0149	-.0149
	.0361	.0183	-.0183
	.0483	.0207	-.0207
	.0604	.0228	-.0228
	.0909	.0264	-.0264
	.1216	.0285	-.0285
	.1525	.0292	-.0292
	.1837	.0284	-.0284
	.2150	.0264	-.0264
	.2466	.0234	-.0234
	.2784	.0196	-.0196
	.3104	.0152	-.0152
	.3426	.0106	-.0106
	.3751	.0062	-.0062
	.4078	.0014	-.0014
	.4170	.0001	-.0001

TABLE I.- WING ORDINATES - Continued

(a) Flat wing, wing thickness I (thick) - Concluded

$\frac{\rho}{b/2}$	$\frac{\sigma}{b/2}$	$\frac{z_U}{b/2}$	$\frac{z_L}{b/2}$
2.6	0	0	0
	.0130	.0107	-.0107
	.0261	.0151	-.0151
	.0392	.0183	-.0183
	.0523	.0207	-.0207
	.0654	.0226	-.0226
	.0985	.0259	-.0259
	.1318	.0274	-.0274
	.1653	.0270	-.0270
	.1990	.0251	-.0251
	.2330	.0219	-.0219
	.2671	.0176	-.0176
	.3016	.0129	-.0129
	.3363	.0079	-.0079
	.3711	.0031	-.0031
	.3918	.0001	-.0001
2.8	0	0	0
	.0140	.0107	-.0107
	.0281	.0152	-.0152
	.0422	.0183	-.0183
	.0563	.0206	-.0206
	.0705	.0224	-.0224
	.1061	.0251	-.0251
	.1419	.0256	-.0256
	.1780	.0240	-.0240
	.2143	.0207	-.0207
	.2509	.0161	-.0161
	.2877	.0109	-.0109
	.3248	.0057	-.0057
	.3621	.0003	-.0003
	.3637	.0001	-.0001
3.0	0	0	0
	.0150	.0106	-.0106
	.0301	.0148	-.0148
	.0452	.0177	-.0177
	.0603	.0197	-.0197
	.0755	.0213	-.0213
	.1136	.0231	-.0231
	.1520	.0222	-.0222
	.1907	.0191	-.0191
	.2296	.0144	-.0144
	.2688	.0089	-.0089
	.3083	.0033	-.0033
	.3311	.0001	-.0001
3.2	0	0	0
	.0160	.0096	-.0096
	.0321	.0134	-.0134
	.0482	.0159	-.0159
	.0643	.0176	-.0176
	.0805	.0187	-.0187
	.1212	.0191	-.0191
	.1622	.0165	-.0165
	.2034	.0119	-.0119
	.2449	.0063	-.0063
	.2867	.0008	-.0008
	.2920	.0001	-.0001
3.4	0	0	0
	.0170	.0080	-.0080
	.0341	.0108	-.0108
	.0512	.0127	-.0127
	.0684	.0138	-.0138
	.0856	.0142	-.0142
	.1288	.0126	-.0126
	.1723	.0084	-.0084
	.2161	.0032	-.0032
	.2427	.0001	-.0001
3.6	0	0	0
	.0180	.0059	-.0059
	.0361	.0078	-.0078
	.0542	.0087	-.0087
	.0724	.0087	-.0087
	.0906	.0079	-.0079
	.1364	.0040	-.0040
	.1756	0	0
3.8	0	0	0
	.0190	.0027	-.0027
	.0381	.0022	-.0022
	.0572	.0007	-.0007
	.0650	0	0
3.864	0	0	0

TABLE I.- WING ORDINATES - Continued

(b) Flat wing, wing thickness II (thin)

$\frac{\rho}{b/2}$	$\frac{\sigma}{b/2}$	$\frac{z_U}{b/2}$	$\frac{z_L}{b/2}$
0	0	0	0
0.2	0	0	0
	.0010	.0022	-.0022
	.0030	.0034	-.0034
	.0050	.0044	-.0044
	.0101	.0061	-.0061
	.0153	.0074	-.0074
	.0206	.0086	-.0086
	.0259	.0095	-.0095
	.0313	.0104	-.0104
	.0367	.0112	-.0112
	.0423	.0121	-.0121
	.0479	.0129	-.0129
	.0536	.0138	-.0138
0.4	0	0	0
	.0020	.0030	-.0030
	.0040	.0042	-.0042
	.0080	.0056	-.0056
	.0101	.0064	-.0064
	.0203	.0090	-.0090
	.0254	.0101	-.0101
	.0358	.0118	-.0118
	.0411	.0127	-.0127
	.0464	.0134	-.0134
	.0571	.0147	-.0147
	.0680	.0161	-.0161
	.0734	.0167	-.0167
	.0790	.0173	-.0173
	.0901	.0181	-.0181
	.1072	.0194	-.0194
0.6	0	0	0
	.0030	.0036	-.0036
	.0060	.0051	-.0051
	.0090	.0062	-.0062
	.0151	.0080	-.0080
	.0227	.0097	-.0097
	.0381	.0127	-.0127
	.0459	.0138	-.0138
	.0696	.0166	-.0166
	.0776	.0174	-.0174
	.0857	.0182	-.0182
	.1019	.0194	-.0194
	.1102	.0200	-.0200
	.1268	.0209	-.0209
	.1352	.0214	-.0214
	.1436	.0218	-.0218
	.1522	.0222	-.0222
	.1608	.0225	-.0225

$\frac{\rho}{b/2}$	$\frac{\sigma}{b/2}$	$\frac{z_U}{b/2}$	$\frac{z_L}{b/2}$
0.8	0	0	0
	.0040	.0040	-.0040
	.0080	.0056	-.0056
	.0160	.0082	-.0082
	.0201	.0092	-.0092
	.0303	.0112	-.0112
	.0508	.0143	-.0143
	.0612	.0156	-.0156
	.0717	.0168	-.0168
	.0927	.0186	-.0186
	.1035	.0195	-.0195
	.1142	.0202	-.0202
	.1359	.0213	-.0213
	.1469	.0218	-.0218
	.1691	.0225	-.0225
	.1803	.0228	-.0228
	.2029	.0231	-.0231
	.2143	.0231	-.0231
1.0	0	0	0
	.0050	.0044	-.0044
	.0100	.0062	-.0062
	.0151	.0076	-.0076
	.0252	.0099	-.0099
	.0379	.0121	-.0121
	.0507	.0140	-.0140
	.0765	.0166	-.0166
	.0896	.0176	-.0176
	.1028	.0186	-.0186
	.1293	.0203	-.0203
	.1428	.0208	-.0208
	.1563	.0213	-.0213
	.1836	.0219	-.0219
	.1974	.0221	-.0221
	.2113	.0221	-.0221
	.2394	.0217	-.0217
	.2679	.0209	-.0209
1.2	0	0	0
	.0060	.0046	-.0046
	.0120	.0067	-.0067
	.0180	.0081	-.0081
	.0241	.0093	-.0093
	.0455	.0128	-.0128
	.0608	.0147	-.0147
	.0918	.0173	-.0173
	.1076	.0184	-.0184
	.1233	.0192	-.0192
	.1552	.0202	-.0202
	.1713	.0207	-.0207
	.1875	.0209	-.0209
	.2203	.0207	-.0207
	.2369	.0204	-.0204
	.2535	.0200	-.0200
	.3043	.0178	-.0178
	.3215	.0168	-.0168

TABLE I.- WING ORDINATES - Continued

(b) Flat wing, wing thickness II (thin) - Continued

$\frac{\rho}{b/2}$	$\frac{\sigma}{b/2}$	$\frac{z_U}{b/2}$	$\frac{z_L}{b/2}$
1.4	0	0	0
	.0070	.0050	-.0050
	.0140	.0072	-.0072
	.0211	.0086	-.0086
	.0282	.0099	-.0099
	.0352	.0110	-.0110
	.0710	.0153	-.0153
	.0890	.0169	-.0169
	.1254	.0188	-.0188
	.1439	.0196	-.0196
	.1811	.0201	-.0201
	.1999	.0202	-.0202
	.2188	.0200	-.0202
	.2571	.0191	-.0200
	.2764	.0181	-.0181
	.3155	.0157	-.0157
	.3551	.0130	-.0130
	.3751	.0117	-.0117
1.6	0	0	0
	.0080	.0056	-.0056
	.0160	.0076	-.0076
	.0240	.0094	-.0094
	.0322	.0109	-.0109
	.0403	.0121	-.0121
	.0606	.0146	-.0146
	.1017	.0179	-.0179
	.1225	.0190	-.0190
	.1434	.0197	-.0197
	.1644	.0202	-.0202
	.1856	.0203	-.0203
	.2069	.0201	-.0201
	.2501	.0188	-.0188
	.2718	.0179	-.0179
	.2938	.0167	-.0167
	.3381	.0134	-.0134
	.3605	.0117	-.0117
	.4058	.0080	-.0080
	.4287	.0062	-.0062
1.8	0	0	0
	.0090	.0060	-.0060
	.0180	.0086	-.0086
	.0281	.0105	- 0105
	.0456	.0136	-.0136
	.0682	.0161	-.0161
	.0912	.0179	-.0179
	.1144	.0192	-.0192
	.1378	.0203	-.0203
	.1613	.0208	-.0208
	.1850	.0207	-.0207
	.2328	.0194	-.0194
	.2570	.0185	-.0185
	.3058	.0153	-.0153
	.3554	.0112	-.0112
	.3804	.0091	-.0091
	.4056	.0069	-.0069
	.4310	.0047	-.0047
	.4566	.0025	-.0025
	.4823	.0002	-.0002

$\frac{\rho}{b/2}$	$\frac{\sigma}{b/2}$	$\frac{z_U}{b/2}$	$\frac{z_L}{b/2}$
2.0	0	0	0
	.0100	.0069	-.0069
	.0200	.0095	-.0095
	.0301	.0117	-.0117
	.0402	.0134	-.0134
	.0758	.0176	-.0176
	.1014	.0194	-.0194
	.1271	.0208	-.0208
	.1531	.0213	-.0213
	.1792	.0214	-.0214
	.2055	.0209	-.0209
	.2320	.0197	-.0197
	.2587	.0182	-.0182
	.2855	.0161	-.0161
	.3126	.0140	-.0140
	.3398	.0115	-.0115
	.3672	.0088	-.0088
	.3948	.0063	-.0063
	.4227	.0036	-.0036
	.4620	.0001	-.0001
2.2	0	0	0
	.0110	.0074	-.0074
	.0221	.0102	-.0102
	.0331	.0124	-.0124
	.0442	.0141	-.0141
	.0554	.0156	-.0156
	.0833	.0183	-.0183
	.1115	.0200	-.0200
	.1398	.0209	-.0209
	.1684	.0211	-.0211
	.1971	.0205	-.0205
	.2261	.0193	-.0193
	.2552	.0173	-.0173
	.2845	.0149	-.0149
	.3141	.0122	-.0122
	.3438	.0094	-.0094
	.3738	.0065	-.0065
	.4039	.0035	-.0035
	.4343	.0005	-.0005
	.4401	.0001	-.0001
2.4	0	0	0
	.0120	.0080	-.0080
	.0241	.0107	-.0107
	.0361	.0129	-.0129
	.0483	.0147	-.0147
	.0604	.0162	-.0162
	.0909	.0188	-.0188
	.1216	.0201	-.0201
	.1526	.0204	-.0204
	.1837	.0200	-.0200
	.2150	.0186	-.0186
	.2466	.0165	-.0165
	.2784	.0137	-.0137
	.3104	.0105	-.0105
	.3426	.0075	-.0075
	.3751	.0042	-.0042
	.4078	.0011	-.0011
	.4150	.0001	-.0001

TABLE I.- WING ORDINATES - Continued

(b) Flat wing, wing thickness II (thin) - Concluded

$\frac{\rho}{b/2}$	$\frac{\sigma}{b/2}$	$\frac{z_U}{b/2}$	$\frac{z_L}{b/2}$
2.6	0	0	0
	.0130	.0076	-.0076
	.0261	.0107	-.0107
	.0392	.0129	-.0129
	.0523	.0146	-.0146
	.0654	.0160	-.0160
	.0985	.0184	-.0184
	.1318	.0193	-.0193
	.1653	.0189	-.0189
	.1990	.0177	-.0177
	.2330	.0155	-.0155
	.2672	.0126	-.0126
	.3016	.0091	-.0091
	.3363	.0056	-.0056
	.3712	.0022	-.0022
	.3918	.0001	-.0001
2.8	0	0	0
	.0140	.0076	-.0076
	.0281	.0108	-.0108
	.0422	.0130	-.0130
	.0563	.0147	-.0147
	.0705	.0160	-.0160
	.1061	.0179	-.0179
	.1419	.0181	-.0181
	.1780	.0171	-.0171
	.2143	.0147	-.0147
	.2509	.0114	-.0114
	.2877	.0077	-.0077
	.3248	.0040	-.0040
	.3621	.0002	-.0002
	.3637	.0001	-.0001
3.0	0	0	0
	.0150	.0075	-.0075
	.0301	.0105	-.0105
	.0452	.0125	-.0125
	.0603	.0140	-.0140
	.0755	.0151	-.0151
	.1136	.0165	-.0165
	.1520	.0157	-.0157
	.1907	.0135	-.0135
	.2296	.0101	-.0101
	.2688	.0064	-.0064
	.3083	.0023	-.0023
	.3311	.0001	-.0001

$\frac{\rho}{b/2}$	$\frac{\sigma}{b/2}$	$\frac{z_U}{b/2}$	$\frac{z_L}{b/2}$
3.2	0	0	0
	.0160	.0068	-.0068
	.0321	.0094	-.0094
	.0482	.0112	-.0112
	.0644	.0125	-.0125
	.0805	.0132	-.0132
	.1212	.0137	-.0137
	.1622	.0117	-.0117
	.2034	.0084	-.0084
	.2449	.0045	-.0045
	.2867	.0005	-.0005
	.2920	.0001	-.0001
3.4	0	0	0
	.0170	.0056	-.0056
	.0341	.0076	-.0076
	.0512	.0090	-.0090
	.0684	.0098	-.0098
	.0856	.0100	-.0100
	.1288	.0089	-.0089
	.1723	.0060	-.0060
	.2161	.0023	-.0023
	.2427	.0001	-.0001
3.6	0	0	0
	.0180	.0042	-.0042
	.0361	.0054	-.0054
	.0542	.0061	-.0061
	.0724	.0062	- 0062
	.0906	.0056	-.0056
	.1364	.0028	-.0028
	.1756	0	0
3.8	0	0	0
	.0190	.0019	-.0019
	.0381	.0016	-.0016
	.0572	.0005	-.0005
	.0650	0	0
3.864	0	0	0

TABLE I.- WING ORDINATES - Continued

(c) Twisted and cambered wing, wing thickness I (thick)

$\frac{\rho}{b/2}$	$\frac{\sigma}{b/2}$	$\frac{z_U}{b/2}$	$\frac{z_L}{b/2}$
0	0	0.2030	0.2030
0.2	0	0.0766	0.0766
	.0010	.0806	.0745
	.0030	.0845	.0748
	.0050	.0879	.0754
	.0101	.0944	.0775
	.0153	.1012	.0802
	.0206	.1078	.0836
	.0259	.1140	.0872
	.0313	.1209	.0914
	.0367	.1284	.0962
	.0423	.1364	.1025
	.0479	.1465	.1099
	.0536	.1595	.1205
0.4	0	0.0396	0.0396
	.0020	.0456	.0371
	.0040	.0488	.0368
	.0080	.0531	.0372
	.0101	.0555	.0375
	.0203	.0641	.0387
	.0254	.0679	.0394
	.0358	.0744	.0409
	.0411	.0775	.0417
	.0464	.0804	.0424
	.0571	.0858	.0441
	.0680	.0911	.0456
	.0734	.0937	.0465
	.0790	.0961	.0473
	.0901	.1000	.0487
	.1072	.1045	.0496
0.6	0	0.0181	0.0181
	.0030	.0257	.0148
	.0060	.0292	.0153
	.0090	.0316	.0146
	.0151	.0365	.0137
	.0227	.0409	.0135
	.0381	.0483	.0129
	.0459	.0511	.0121
	.0696	.0578	.0110
	.0776	.0601	.0108
	.0857	.0616	.0102
	.1019	.0639	.0092
	.1102	.0645	.0080
	.1268	.0636	.0044
	.1352	.0610	.0004
	.1436	.0579	-.0038
	.1522	.0526	-.0110
	.1608	.0465	-.0170

$\frac{\rho}{b/2}$	$\frac{\sigma}{b/2}$	$\frac{z_U}{b/2}$	$\frac{z_L}{b/2}$
0.8	0	0.0083	0.0083
	.0040	.0159	.0041
	.0080	.0193	.0036
	.0160	.0244	.0011
	.0201	.0265	.0009
	.0303	.0305	-.0013
	.0508	.0358	-.0050
	.0612	.0380	-.0062
	.0717	.0394	-.0080
	.0927	.0408	-.0119
	.1035	.0413	-.0138
	.1142	.0414	-.0156
	.1359	.0406	-.0197
	.1469	.0394	-.0223
	.1691	.0360	-.0279
	.1803	.0326	-.0320
	.2029	.0169	-.0485
	.2143	.0079	-.0575
1.0	0	0.0054	0.0054
	.0050	.0134	.0009
	.0100	.0169	-.0008
	.0151	.0197	-.0023
	.0252	.0229	-.0048
	.0379	.0260	-.0084
	.0507	.0279	-.0114
	.0765	.0289	-.0186
	.0896	.0278	-.0227
	.1028	.0275	-.0256
	.1293	.0248	-.0326
	.1428	.0228	-.0362
	.1563	.0214	-.0390
	.1836	.0147	-.0473
	.1974	.0115	-.0510
	.2113	.0075	-.0550
	.2394	-.0035	-.0650
	.2679	-.0215	-.0805
1.2	0	0.0064	0.0064
	.0060	.0150	.0020
	.0120	.0188	-.0001
	.0180	.0213	-.0017
	.0241	.0230	-.0033
	.0455	.0263	-.0100
	.0608	.0259	-.0156
	.0918	.0229	-.0260
	.1075	.0206	-.0314
	.1233	.0177	-.0365
	.1552	.0104	-.0471
	.1713	.0065	-.0520
	.1875	.0020	-.0572
	.2203	-.0088	-.0676
	.2369	-.0142	-.0721
	.2535	-.0211	-.0776
	.3043	-.0436	-.0940
	.3215	-.0504	-.0980

TABLE I.- WING ORDINATES - Continued

(c) Twisted and cambered wing, wing thickness I (thick) - Continued

$\frac{\rho}{b/2}$	$\frac{\sigma}{b/2}$	$\frac{z_U}{b/2}$	$\frac{z_L}{b/2}$
1.4	0	0.0074	0.0074
	.0070	.0168	.0030
	.0140	.0211	.0008
	.0211	.0236	-.0008
	.0282	.0255	-.0026
	.0352	.0269	-.0046
	.0710	.0277	-.0158
	.0890	.0248	-.0226
	.1254	.0166	-.0367
	.1439	.0114	-.0439
	.1811	-.0010	-.0582
	.1999	-.0078	-.0651
	.2188	-.0147	-.0712
	.2571	-.0308	-.0843
	.2764	-.0385	-.0896
	.3155	-.0540	-.0990
	.3551	-.0717	-.1090
	.3751	-.0789	-.1120
1.6	0	0.0084	0.0084
	.0080	.0191	.0033
	.0160	.0233	.0015
	.0240	.0262	-.0003
	.0322	.0284	-.0023
	.0403	.0300	-.0045
	.0606	.0315	-.0098
	.1017	.0267	-.0240
	.1225	.0222	-.0314
	.1434	.0157	-.0401
	.1644	.0079	-.0491
	.1856	-.0008	-.0582
	.2069	-.0101	-.0669
	.2501	-.0302	-.0834
	.2718	-.0409	-.0911
	.2938	-.0511	-.0979
	.3381	-.0700	-.1080
	.3605	-.0800	-.1130
	.4058	-.0972	-.1200
	.4287	-.1039	-.1215
1.8	0	0.0093	0.0093
	.0090	.0210	.0040
	.0180	.0260	.0017
	.0271	.0294	-.0004
	.0453	.0333	-.0047
	.0682	.0351	-.0105
	.0912	.0333	-.0176
	.1144	.0291	-.0257
	.1378	.0238	- 0336
	.1613	.0161	-.0427
	.1850	.0068	-.0522
	.2328	-.0182	-.0737
	.2570	-.0309	-.0833
	.3058	-.0587	-.1020
	.3554	-.0844	-.1160
	.3804	-.0954	-.1210
	.4056	-.1046	-.1240
	.4310	-.1118	-.1250
	.4566	-.1172	-.1250
	.4823	-.1224	-.1230

$\frac{\rho}{b/2}$	$\frac{\sigma}{b/2}$	$\frac{z_U}{b/2}$	$\frac{z_L}{b/2}$
2.0	0	0.0103	0.0103
	.0100	.0235	.0041
	.0200	.0287	.0019
	.0301	.0325	-.0005
	.0402	.0352	-.0028
	.0758	.0385	-.0110
	.1014	.0364	-.0186
	.1271	.0315	-.0271
	.1531	.0252	-.0351
	.1792	.0161	-.0443
	.2055	.0049	-.0539
	.2320	-.0091	-.0648
	.2587	-.0248	-.0762
	.2855	-.0413	-.0872
	.3126	-.0583	-.0978
	.3398	-.0761	-.1085
	.3672	-.0927	-.1180
	.3948	-.1060	-.1240
	.4227	-.1164	-.1270
	.4620	- 1298	-.1300
2.2	0	0.0111	0.0111
	.0110	.0254	.0046
	.0221	.0311	.0023
	.0331	.0350	0
	.0442	.0378	-.0022
	.0554	.0396	-.0046
	.0833	.0412	-.0105
	.1115	.0385	-.0181
	.1398	.0326	-.0267
	.1684	.0252	-.0346
	.1971	.0145	-.0435
	.2261	.0014	-.0531
	.2552	-.0148	-.0640
	.2845	-.0329	-.0753
	.3141	-.0520	-.0868
	.3438	-.0725	-.0992
	.3738	-.0930	-.1115
	.4039	-.1124	-.1226
	.4343	-.1273	- 1290
	.4401	-.1309	-.1311
2.4	0	0.0120	0.0120
	.0120	.0275	.0047
	.0241	.0329	.0031
	.0361	.0372	.0007
	.0483	.0401	-.0014
	.0604	.0417	-.0038
	.0909	.0435	-.0094
	.1216	.0401	-.0169
	.1526	.0331	-.0252
	.1837	.0242	-.0325
	.2150	.0119	-.0410
	.2466	-.0034	-.0501
	.2784	-.0218	-.0609
	.3104	-.0420	-.0723
	.3426	-.0626	-.0838
	.3751	-.0858	-.0982
	.4078	-.1092	-.1120
	.4170	-.1158	-.1160

TABLE I.- WING ORDINATE - Continued

(c) Twisted and cambered wing, wing thickness I (thick) - Concluded

$\frac{\rho}{b/2}$	$\frac{\sigma}{b/2}$	$\frac{z_U}{b/2}$	$\frac{z_L}{b/2}$
2.6	0	0.0128	0.0128
	.0130	.0279	.0065
	.0261	.0344	.0042
	.0392	.0386	.0021
	.0523	.0416	.0002
	.0654	.0433	-.0018
	.0985	.0448	-.0071
	.1318	.0407	-.0141
	.1653	.0323	-.0218
	.1990	.0219	-.0283
	.2330	.0078	-.0360
	.2672	-.0095	-.0448
	.3016	-.0298	-.0556
	.3363	-.0516	-.0675
	.3712	-.0736	-.0799
	.3918	-.0879	-.0881
2.8	0	0.0135	0.0135
	.0140	.0289	.0075
	.0281	.0358	.0053
	.0422	.0401	.0034
	.0563	.0431	.0019
	.0705	.0448	0
	.1061	.0459	-.0043
	.1419	.0408	-.0104
	.1780	.0309	-.0171
	.2143	.0189	-.0226
	.2509	.0030	-.0292
	.2877	-.0161	-.0379
	.3248	-.0378	-.0491
	.3621	-.0610	-.0616
	.3637	-.0619	- 0621
3.0	0	0.0141	0.0141
	.0150	.0297	.0086
	.0301	.0365	.0069
	.0452	.0408	.0055
	.0603	.0438	.0043
	.0755	.0455	.0029
	.1136	.0461	-.0002
	.1520	.0396	-.0049
	.1907	.0281	-.0102
	.2296	.0144	-.0143
	.2688	-.0026	-.0204
	.3083	-.0228	-.0295
	.3311	-.0349	-.0351

$\frac{\rho}{b/2}$	$\frac{\sigma}{b/2}$	$\frac{z_U}{b/2}$	$\frac{z_L}{b/2}$
3.2	0	0.0147	0.0147
	.0160	.0297	.0104
	.0321	.0362	.0094
	.0482	.0403	.0086
	.0644	.0432	.0081
	.0805	.0446	.0073
	.1212	.0443	.0062
	.1622	.0364	.0033
	.2034	.0242	.0004
	.2449	.0088	-.0039
	.2867	-.0086	-.0101
	.2920	-.0099	-.0101
3.4	0	0.0153	0.0153
	.0170	.0288	.0128
	.0341	.0344	.0131
	.0512	.0385	.0130
	.0684	.0410	.0134
	.0856	.0420	.0136
	.1288	.0402	.0150
	.1723	.0310	.0142
	.2161	.0175	.0111
	.2427	.0091	.0089
3.6	0	0.0157	0.0157
	.0180	.0274	.0155
	.0361	.0326	.0170
	.0542	.0356	.0183
	.0724	.0375	.0201
	.0906	.0376	.0217
	.1364	.0345	.0265
	.1756	.0258	.0258
3.8	0	0.0161	0.0161
	.0190	.0247	.0194
	.0381	.0279	.0235
	.0572	.0288	.0275
	.0650	.0290	.0290
3.864	0	0.0162	0.0162

TABLE I.- WING ORDINATES - Continued

(d) Twisted and cambered wing, wing thickness II (thin)

$\frac{\rho}{b/2}$	$\frac{\sigma}{b/2}$	$\frac{z_U}{b/2}$	$\frac{z_L}{b/2}$
0	0	0.2030	0.2030
0.2	0	0.0766	0.0766
	.0010	.0798	.0754
	.0030	.0831	.0763
	.0050	.0861	.0773
	.0101	.0921	.0799
	.0153	.0981	.0833
	.0206	.1043	.0871
	.0259	.1101	.0911
	.0313	.1166	.0958
	.0367	.1235	.1011
	.0423	.1316	.1074
	.0479	.1411	.1153
	.0536	.1538	.1262
0.4	0	0.0396	0.0396
	.0020	.0444	.0384
	.0040	.0470	.0386
	.0080	.0508	.0396
	.0101	.0529	.0401
	.0203	.0604	.0424
	.0254	.0638	.0436
	.0358	.0695	.0459
	.0411	.0723	.0469
	.0464	.0748	.0480
	.0571	.0797	.0503
	.0680	.0845	.0523
	.0734	.0868	.0534
	.0790	.0890	.0544
	.0901	.0925	.0563
	.1072	.0965	.0577
0.6	0	0.0181	0.0181
	.0030	.0242	.0170
	.0060	.0271	.0169
	.0090	.0293	.0169
	.0151	.0333	.0173
	.0227	.0369	.0175
	.0381	.0431	.0177
	.0459	.0454	.0178
	.0696	.0512	.0180
	.0776	.0528	.0180
	.0857	.0542	.0178
	.1019	.0559	.0171
	.1102	.0563	.0163
	.1268	.0548	.0130
	.1352	.0523	.0095
	.1436	.0485	.0049
	.1522	.0433	-.0011
	.1608	.0373	-.0077

$\frac{\rho}{b/2}$	$\frac{\sigma}{b/2}$	$\frac{z_U}{b/2}$	$\frac{z_L}{b/2}$
0.8	0	0.0083	0.0083
	.0040	.0143	.0063
	.0080	.0170	.0058
	.0160	.0211	.0047
	.0201	.0227	.0043
	.0303	.0258	.0034
	.0508	.0299	.0013
	.0612	.0313	.0001
	.0717	.0324	-.0012
	.0927	.0331	-.0041
	.1035	.0333	-.0057
	.1142	.0331	-.0073
	.1359	.0318	-.0108
	.1469	.0307	-.0129
	.1691	.0264	-.0186
	.1803	.0228	-.0228
	.2029	.0090	-.0372
	.2143	-.0017	-.0479
1.0	0	0.0054	0.0054
	.0050	.0116	.0028
	.0100	.0142	.0018
	.0151	.0160	.0008
	.0252	.0189	-.0009
	.0379	.0210	-.0032
	.0507	.0222	-.0058
	.0765	.0217	-.0115
	.0896	.0208	-.0144
	.1028	.0196	-.0176
	.1293	.0163	-.0244
	.1428	.0142	-.0274
	.1563	.0117	-.0309
	.1836	.0058	-.0380
	.1974	.0023	-.0419
	.2113	-.0017	-.0459
	.2394	-.0126	-.0560
	.2679	-.0301	-.0719
1.2	0	0.0064	0.0064
	.0060	.0131	.0039
	.0120	.0161	.0027
	.0180	.0179	.0017
	.0241	.0192	.0006
	.0455	.0210	-.0046
	.0608	.0201	-.0093
	.0918	.0157	-.0189
	.1075	.0130	-.0238
	.1233	.0097	-.0287
	.1552	.0020	-.0384
	.1713	-.0021	-.0435
	.1875	-.0068	-.0486
	.2203	-.0173	-.0587
	.2369	-.0231	-.0639
	.2535	-.0294	-.0694
	.3043	-.0501	-.0857
	.3215	-.0574	-.0910

TABLE I.- WING ORDINATES - Continued

(d) Twisted and cambered wing, wing thickness II (thin) - Continued

$\frac{\rho}{b/2}$	$\frac{\sigma}{b/2}$	$\frac{z_U}{b/2}$	$\frac{z_L}{b/2}$
1.4	0	0.0070	0.0070
	.0070	.0144	.0044
	.0140	.0178	.0034
	.0211	.0196	.0024
	.0282	.0210	.0012
	.0352	.0218	-.0002
	.0710	.0207	-.0099
	.0890	.0178	-.0160
	.1254	.0083	-.0293
	.1439	.0029	-.0363
	.1811	-.0100	-.0502
	.1999	-.0166	-.0569
	.2188	-.0237	-.0637
	.2571	-.0387	-.0769
	.2764	-.0464	-.0826
	.3155	-.0617	-.0931
	.3551	-.0769	-.1029
	.3751	-.0842	-.1076
1.6	0	0.0073	0.0073
	.0080	.0157	.0045
	.0160	.0188	.0036
	.0240	.0213	.0025
	.0322	.0229	.0011
	.0403	.0239	-.0003
	.0606	.0243	-.0049
	.1017	.0187	-.0171
	.1225	.0133	-.0247
	.1434	.0063	-.0331
	.1644	-.0017	-.0421
	.1856	-.0103	-.0509
	.2069	-.0195	-.0597
	.2501	-.0391	-.0767
	.2718	-.0489	-.0847
	.2938	-.0585	-.0919
	.3381	-.0770	-.1038
	.3605	-.0859	-.1093
	.4058	-.1017	-.1177
	.4287	-.1076	-.1200
1.8	0	0.0067	0.0067
	.0090	.0159	.0039
	.0180	.0199	.0028
	.0281	.0224	.0014
	.0456	.0255	-.0017
	.0682	.0257	-.0065
	.0912	.0232	-.0126
	.1144	.0186	-.0198
	.1378	.0127	-.0279
	.1613	.0050	-.0367
	.1850	-.0048	-.0462
	.2328	-.0285	-.0673
	.2570	-.0413	-.0783
	.3058	-.0677	-.0983
	.3554	-.0916	-.1140
	.3804	-.1016	-.1199
	.4056	-.1100	-.1238
	.4310	-.1165	-.1259
	.4566	-.1214	-.1264
	.4823	-.1251	-.1254

$\frac{\rho}{b/2}$	$\frac{\sigma}{b/2}$	$\frac{z_U}{b/2}$	$\frac{z_L}{b/2}$
2.0	0	0.0054	0.0054
	.0100	.0158	.0020
	.0200	.0199	.0009
	.0301	.0228	-.0006
	.0402	.0248	-.0020
	.0758	.0264	-.0088
	.1014	.0235	-.0153
	.1271	.0185	-.0231
	.1531	.0114	-.0312
	.1792	.0024	-.0404
	.2055	-.0086	-.0504
	.2320	-.0222	-.0616
	.2587	-.0372	-.0736
	.2855	-.0529	-.0851
	.3126	-.0693	-.0973
	.3398	-.0857	-.1087
	.3672	-.1012	-.1188
	.3948	-.1133	-.1259
	.4227	-.1232	-.1304
	.4620	-.1347	-.1349
2.2	0	0.0034	0.0034
	.0110	.0147	-.0001
	.0221	.0192	-.0012
	.0331	.0222	-.0026
	.0442	.0242	-.0040
	.0554	.0254	-.0058
	.0833	.0257	-.0109
	.1115	.0225	-.0175
	.1398	.0168	-.0250
	.1684	.0087	-.0335
	.1971	-.0017	-.0427
	.2261	-.0143	-.0529
	.2552	-.0297	-.0643
	.2845	-.0468	-.0766
	.3141	-.0653	-.0897
	.3438	-.0842	-.1030
	.3738	-.1035	-.1165
	.4039	-.1219	-.1289
	.4343	-.1362	-.1372
	.4401	-.1386	-.1388
2.4	0	0.0010	0.0010
	.0120	.0130	-.0030
	.0241	.0176	-.0040
	.0361	.0209	-.0049
	.0483	.0231	-.0063
	.0604	.0244	-.0080
	.0909	.0247	-.0129
	.1216	.0207	-.0195
	.1526	.0139	-.0269
	.1837	.0048	-.0352
	.2150	-.0069	-.0441
	.2466	-.0213	-.0543
	.2784	-.0385	-.0659
	.3104	-.0574	-.0784
	.3426	-.0770	-.0920
	.3751	-.0987	-.1071
	.4078	-.1204	-.1226
	.4150	-.1268	-.1270

TABLE I.- WING ORDINATES - Concluded

(d) Twisted and cambered wing, wing thickness II (thin) - Concluded

$\frac{\rho}{b/2}$	$\frac{\sigma}{b/2}$	$\frac{z_U}{b/2}$	$\frac{z_L}{b/2}$
2.6	0	-0.0019	-0.0019
	.0131	.0101	-.0051
	.0261	.0153	-.0061
	.0392	.0186	-.0072
	.0523	.0208	-.0084
	.0654	.0221	-.0099
	.0985	.0223	-.0145
	.1318	.0180	-.0206
	.1653	.0100	-.0278
	.1990	-.0002	-.0356
	.2330	-.0133	-.0443
	.2672	-.0294	-.0546
	.3016	-.0483	-.0665
	.3363	-.0686	-.0798
	.3712	-.0896	-.0940
	.3918	-.1026	-.1027
2.8	0	-0.0052	-0.0052
	.0140	.0071	-.0081
	.0281	.0127	-.0089
	.0422	.0161	-.0099
	.0563	.0185	-.0109
	.0705	.0198	-.0122
	.1061	.0196	-.0162
	.1419	.0146	-.0216
	.1780	.0056	-.0286
	.2143	-.0059	-.0353
	.2509	-.0204	-.0432
	.2877	-.0380	-.0534
	.3248	-.0582	-.0662
	.3621	-.0798	-.0802
	.3637	-.0806	-.0808
3.0	0	-0.0086	-0.0086
	.0150	.0040	-.0110
	.0301	.0095	-.0116
	.0452	.0130	-.0120
	.0603	.0153	-.0127
	.0755	.0166	-.0135
	.1136	.0165	-.0165
	.1520	.0104	-.0210
	.1907	.0006	-.0264
	.2296	-.0125	-.0327
	.2688	-.0279	-.0407
	.3083	-.0465	-.0511
	.3311	-.0576	-.0578
3.2	0	-0.0125	-0.0125
	.0160	-.0003	-.0139
	.0321	.0049	-.0139
	.0482	.0085	-.0139
	.0644	.0109	-.0141
	.0805	.0120	-.0144
	.1212	.0115	-.0159
	.1622	.0044	-.0190
	.2034	-.0065	-.0233
	.2449	-.0202	-.0292
	.2867	-.0361	-.0371
	.2920	-.0379	-.0381
3.4	0	-0.0166	-0.0166
	.0170	-.0063	-.0166
	.0341	-.0007	-.0159
	.0512	.0029	-.0151
	.0684	.0051	-.0145
	.0856	.0060	-.0140
	.1288	.0046	-.0132
	.1723	-.0032	-.0152
	.2161	-.0153	-.0199
	.2427	-.0228	-.0230
3.6	0	-0.0213	-0.0213
	.0180	-.0113	-.0197
	.0361	-.0069	-.0177
	.0542	-.0039	-.0160
	.0724	-.0021	-.0145
	.0906	-.0017	-.0129
	.1364	-.0037	-.0094
	.1756	-.0102	-.0102
3.8	0	-0.0268	-0.0268
	.0190	-.0189	-.0227
	.0381	-.0156	-.0188
	.0572	-.0142	-.0152
	.0650	-.0139	-.0139
3.864	0	-0.0285	-0.0285

TABLE II.- SUMMARY OF RESULTS

Description of configuration	$C_{D,min}$	C_{L_α}	$(L/D)_{max}$	$C_{L,opt}$	$\frac{dC_m}{dC_L}$	C_{m_α}	R	Remarks
Flat wing, wing thickness I	0.0064	0.0206	7.14	0.0850	-0.1425	-0.0029	1.50×10^6	Natural transition
Flat wing, wing thickness I	0.0078	0.0206	6.52	0.0900	-0.1400	-0.0029	1.50	Fixed transition
Flat wing, wing thickness II	0.0052	0.0214	7.50	0.0825	-0.1500	-0.0033	1.50	Natural transition
Flat wing, wing thickness II	0.0069	0.0216	6.89	0.0840	-0.1425	-0.0030	1.50	Fixed transition
Twisted and cambered wing, wing thickness I	0.0090	0.0207	6.20	0.098	-0.1425	-0.0028	1.50	Natural transition
Twisted and cambered wing, wing thickness I	0.0094	0.0205	5.90	0.108	-0.1375	-0.0026	1.50	Fixed transition
Twisted and cambered wing, wing thickness II	0.0078	0.0214	7.21	0.093	-0.1435	-0.0028	1.50	Natural transition
Twisted and cambered wing, wing thickness II	0.0085	0.0218	6.58	0.093	-0.1500	-0.0029	1.50	Fixed transition

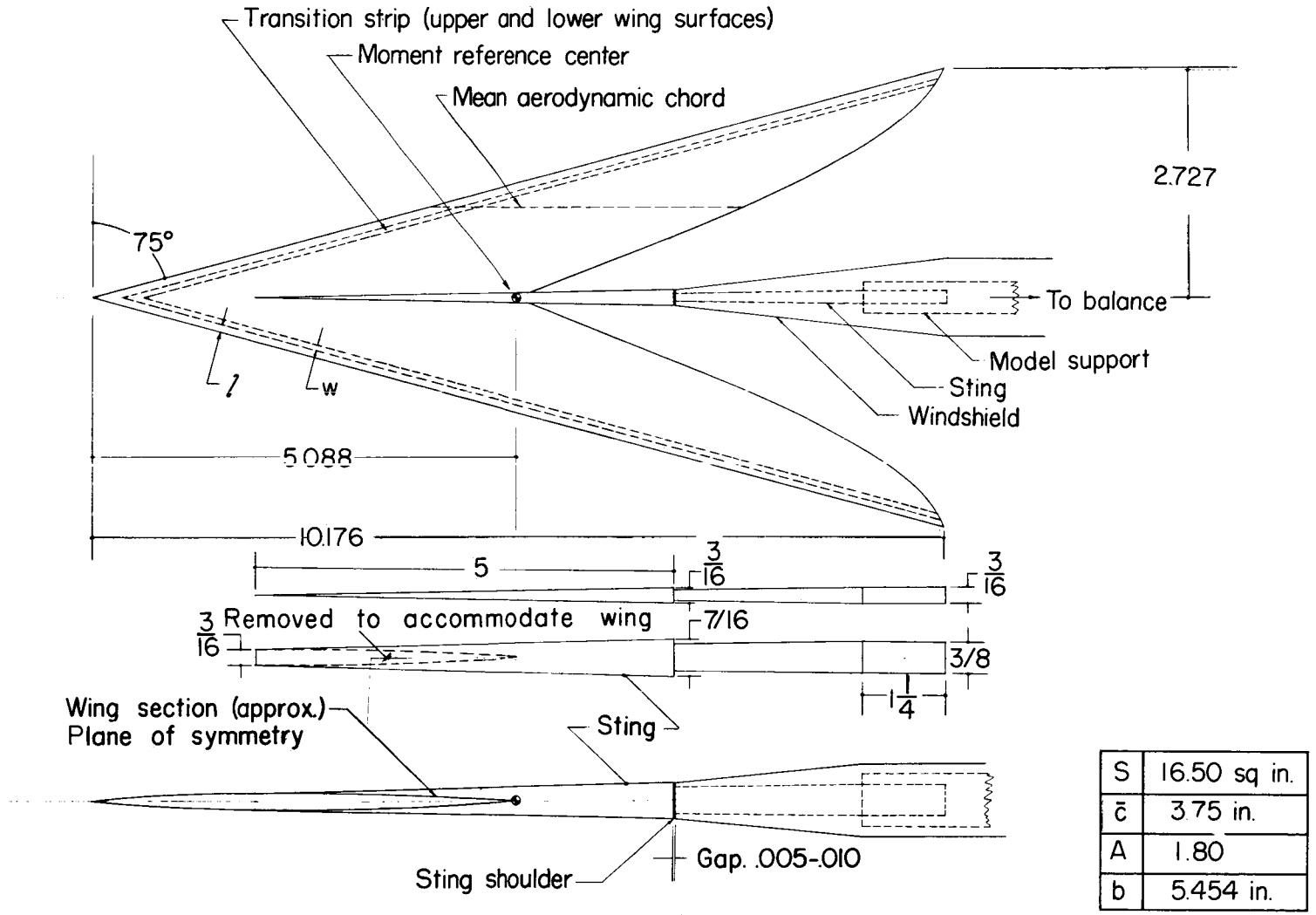

S	16.50 sq in.
$\bar{c}$	3.75 in.
A	1.80
b	5.454 in.

Figure 1.- Dimensional sketch of flat wing showing method of mounting models to model support. Dimensions are in inches.

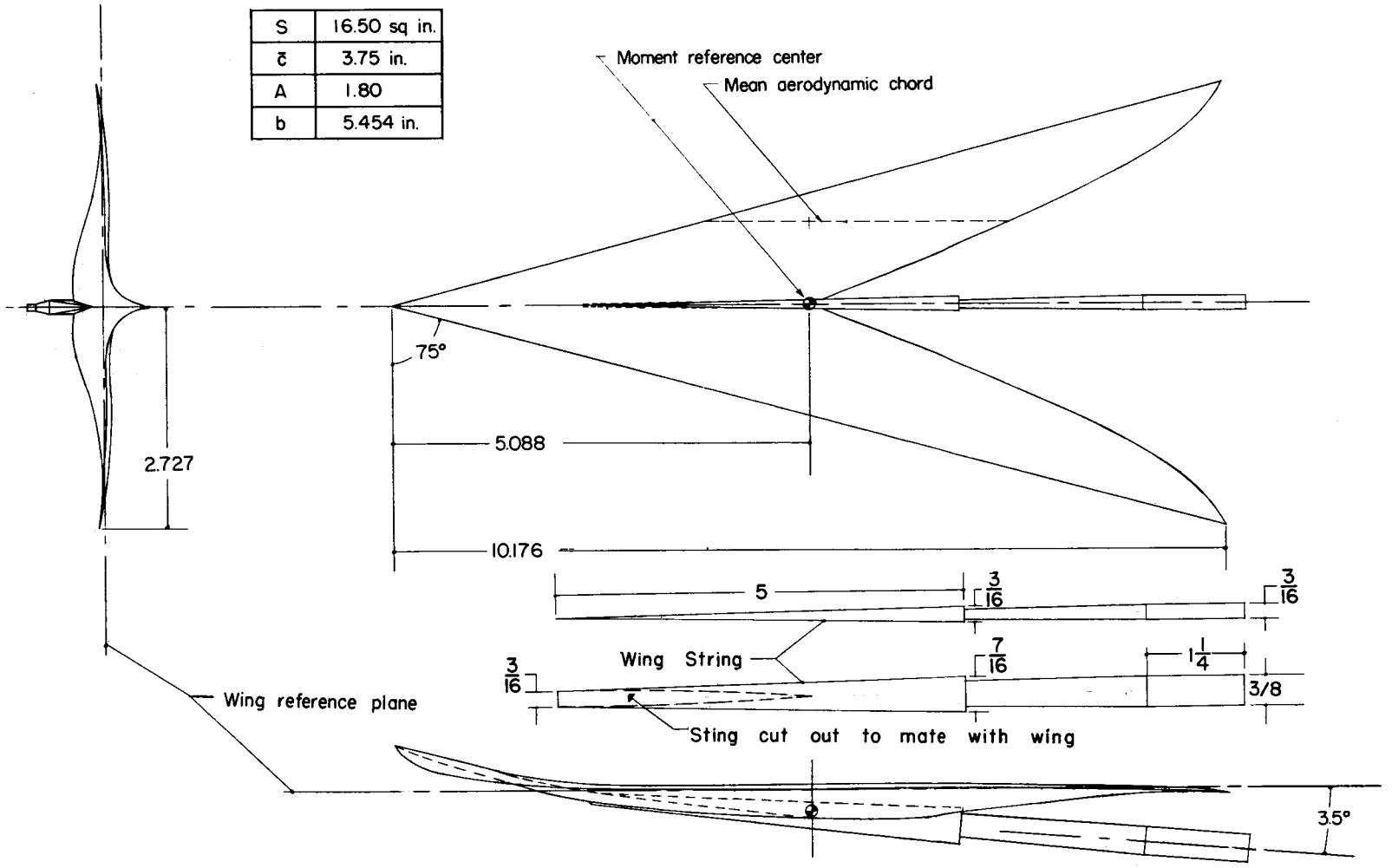

Figure 2.- Dimensional sketch of twisted and cambered wing.

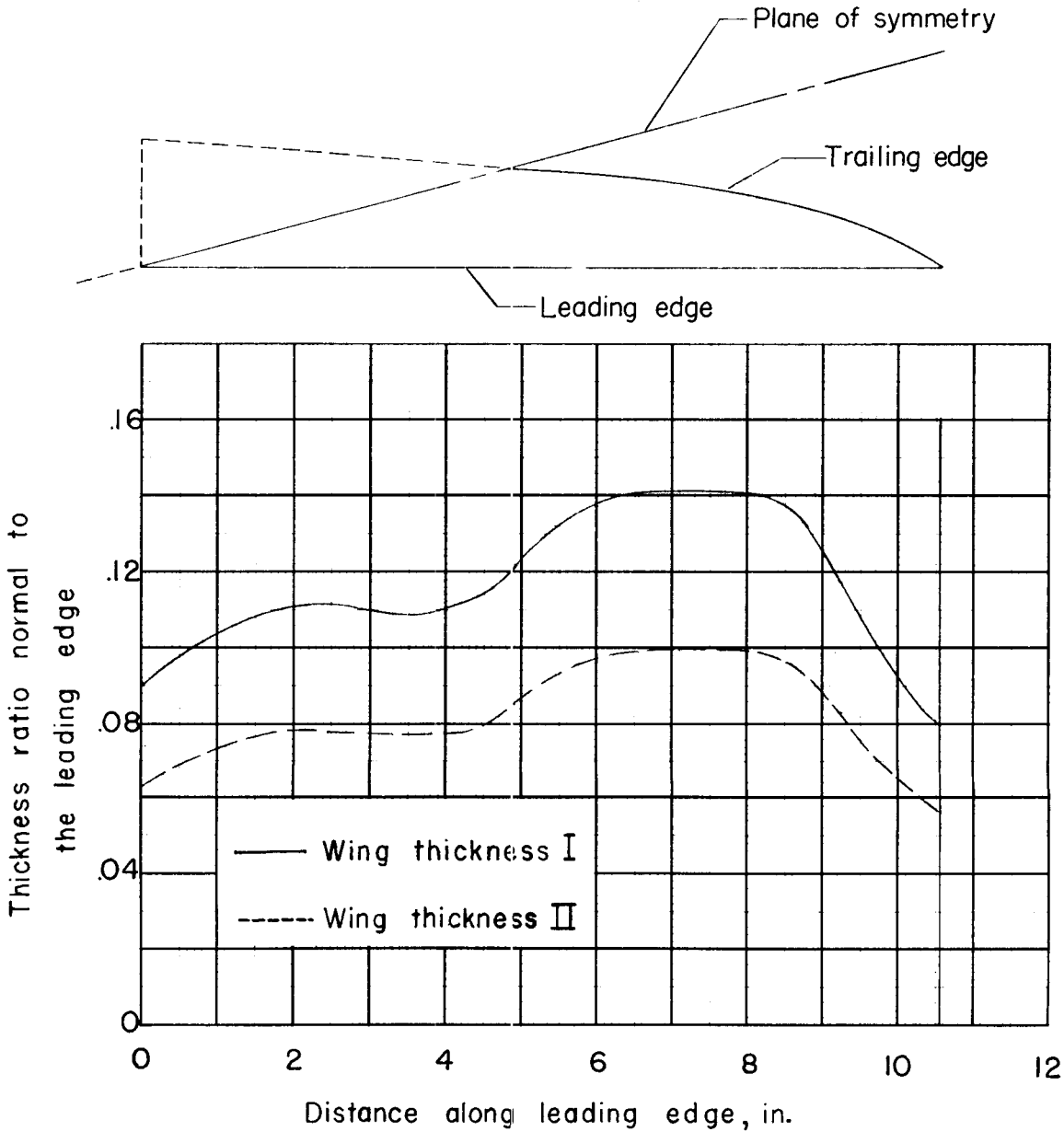

Figure 3.- Thickness distribution of wings.

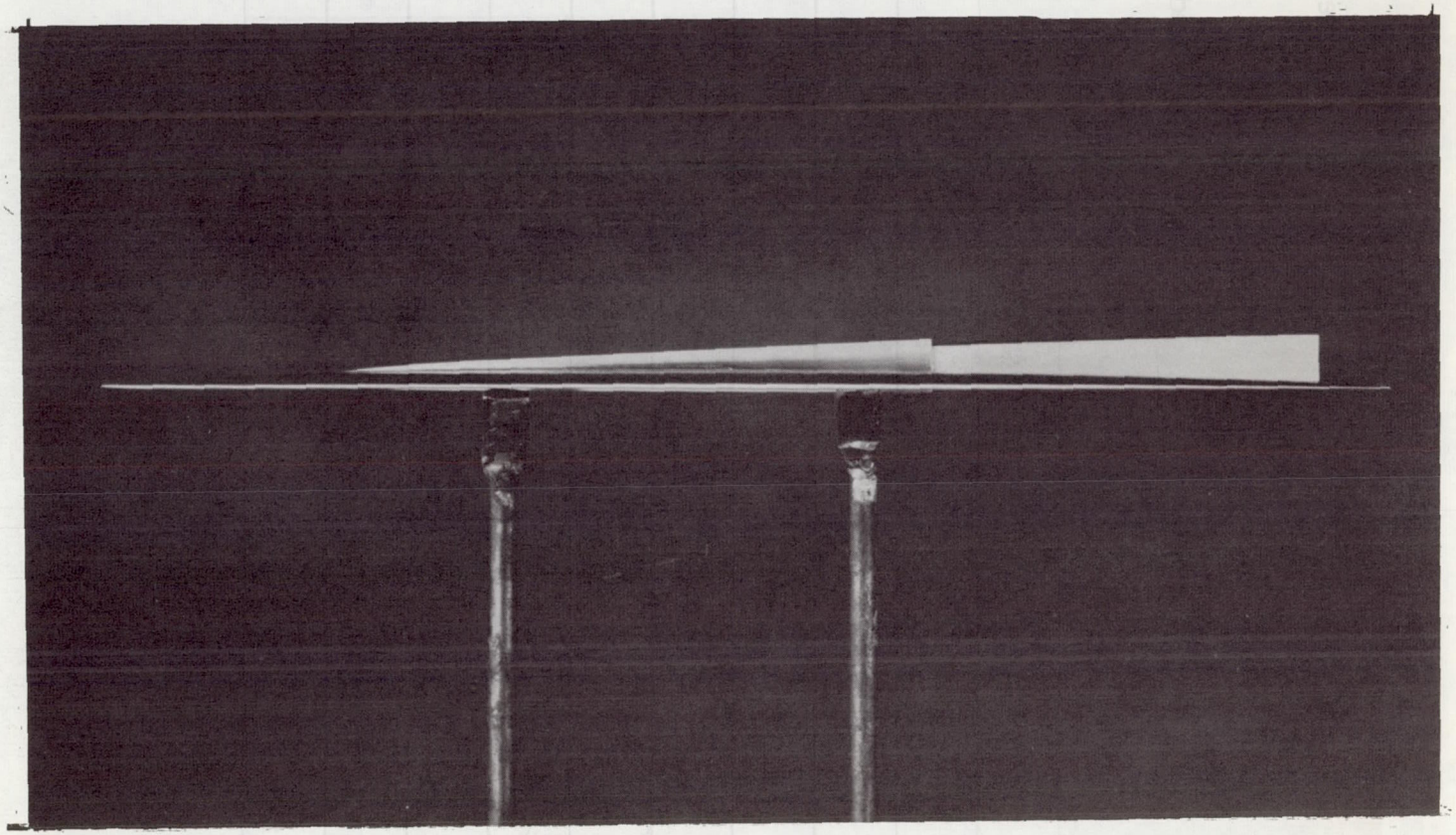

(a) Side view. L-58-3105

Figure 4.- Photographs of flat wing. Wing thickness I.

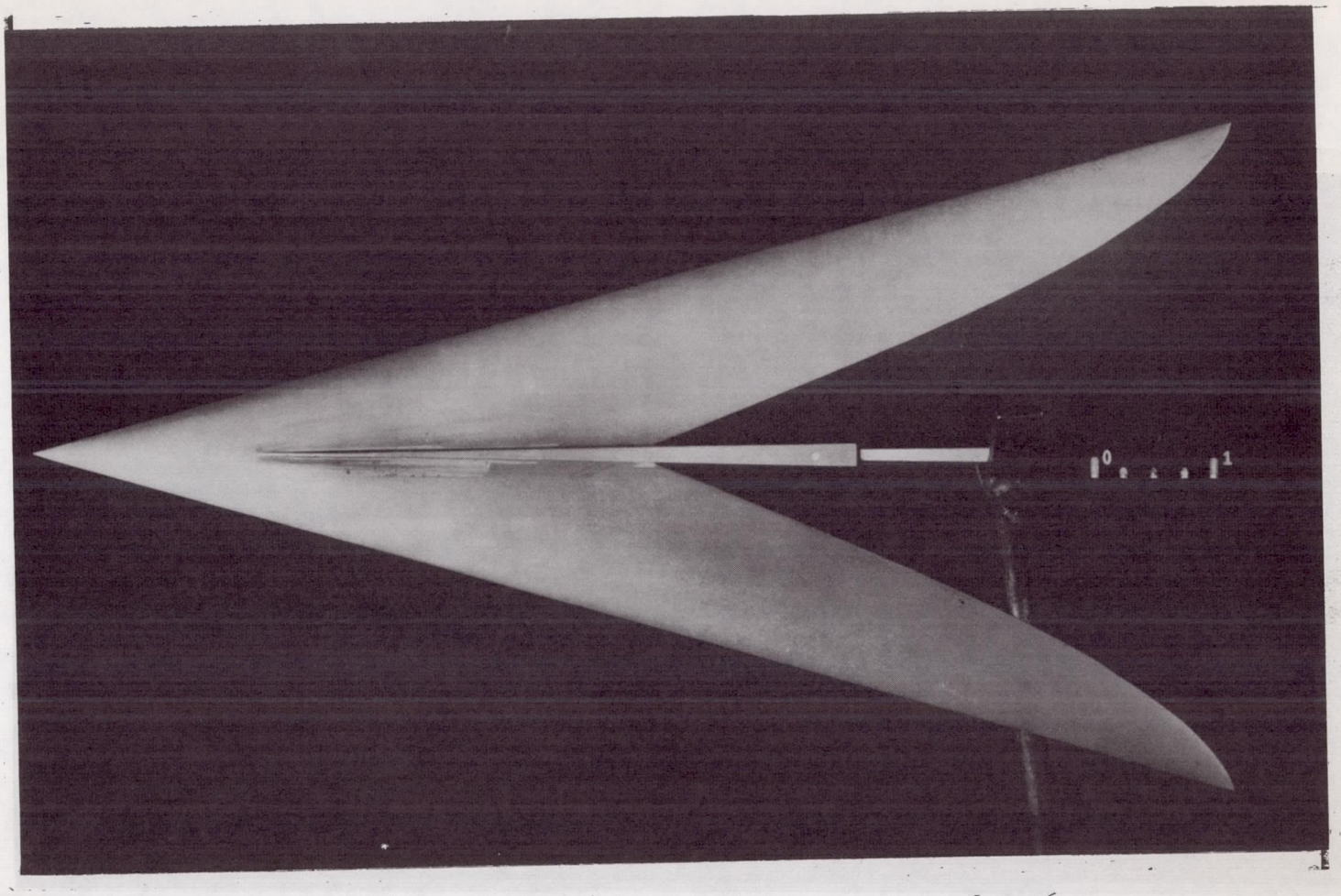

(b) Top view. L-58-3106

Figure 4.- Concluded.

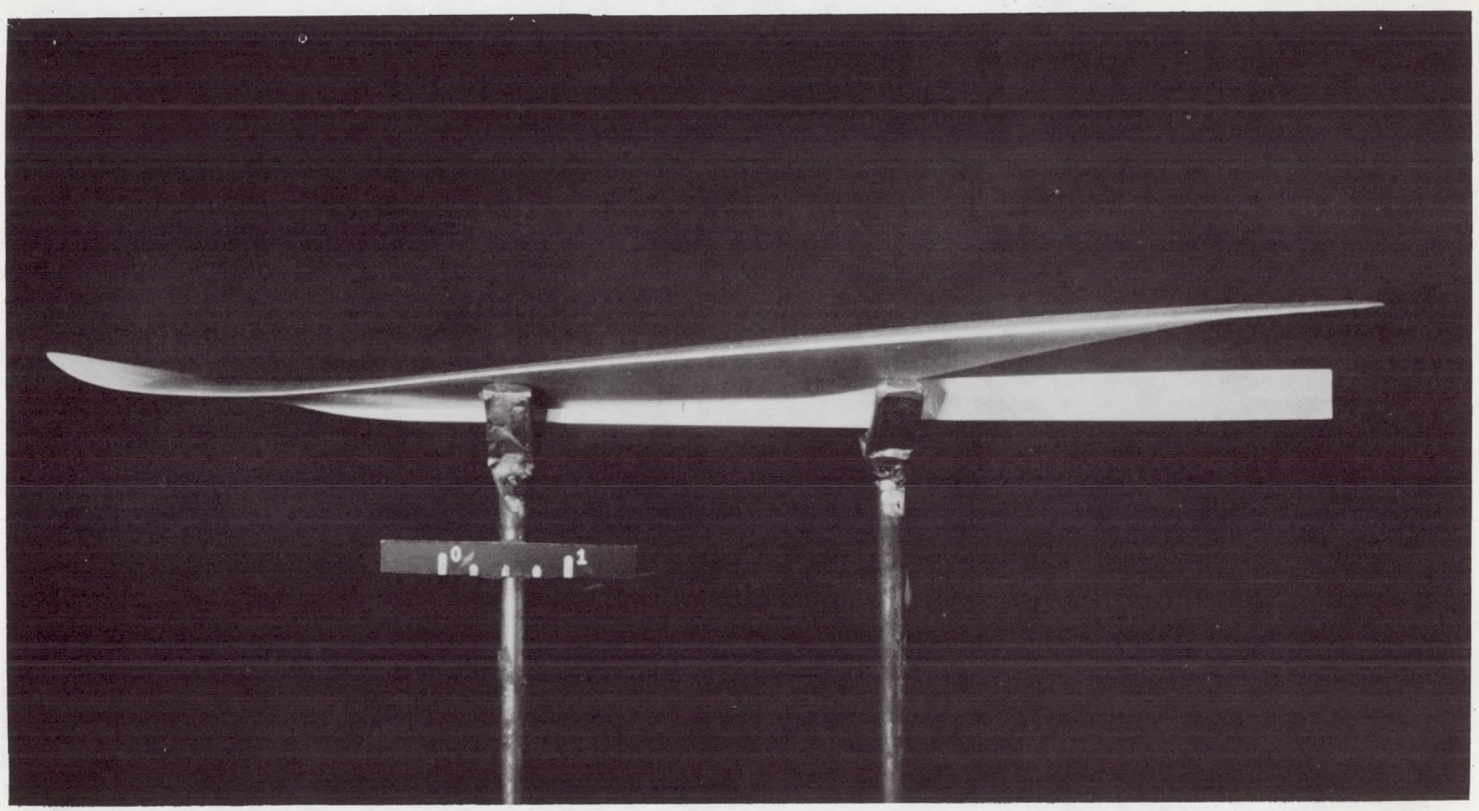

(a) Side view. L-58-2869

Figure 5.- Photographs of twisted and cambered wing. Wing thickness I.

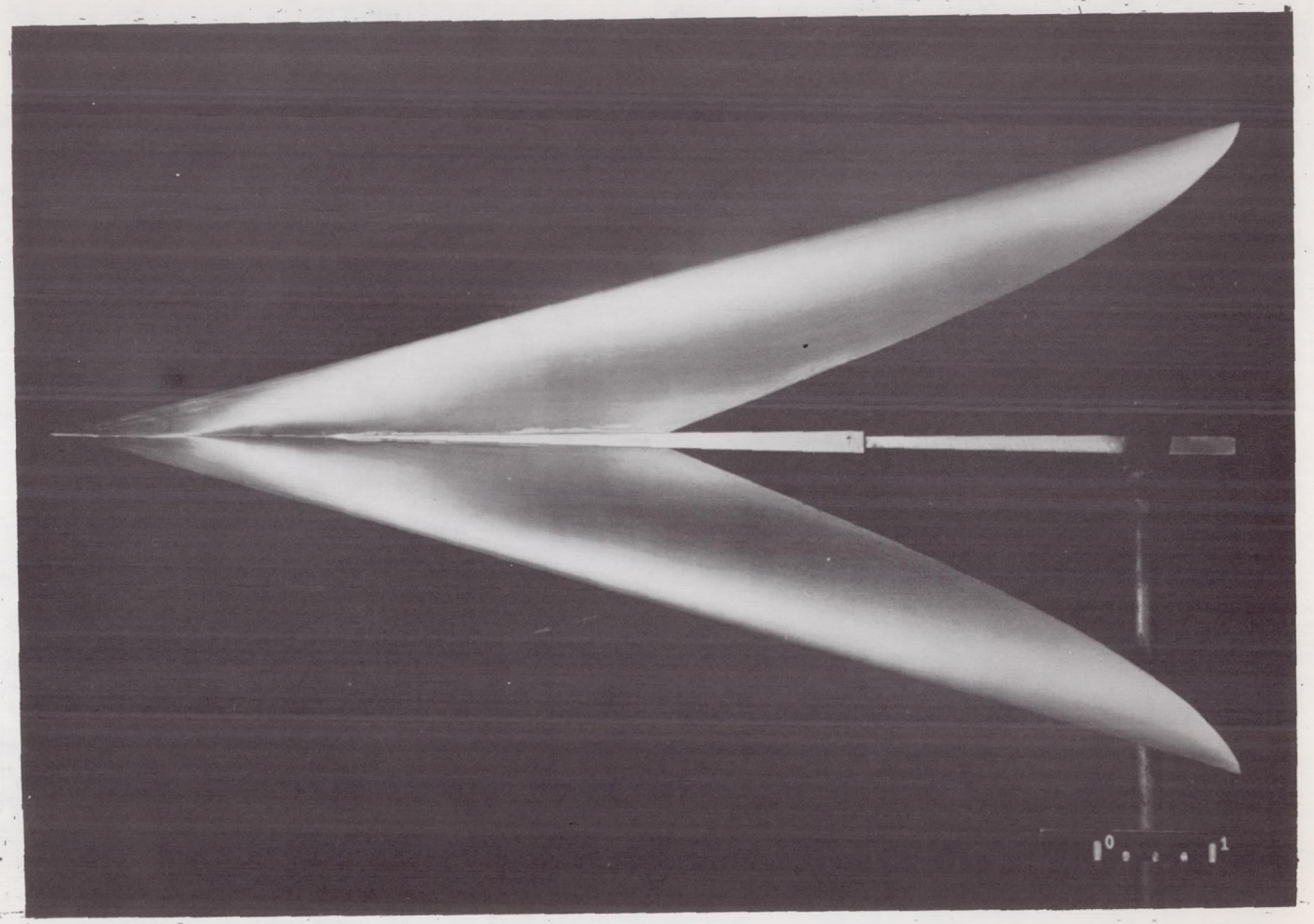

(b) Top view. L-58-2870

Figure 5.- Concluded.

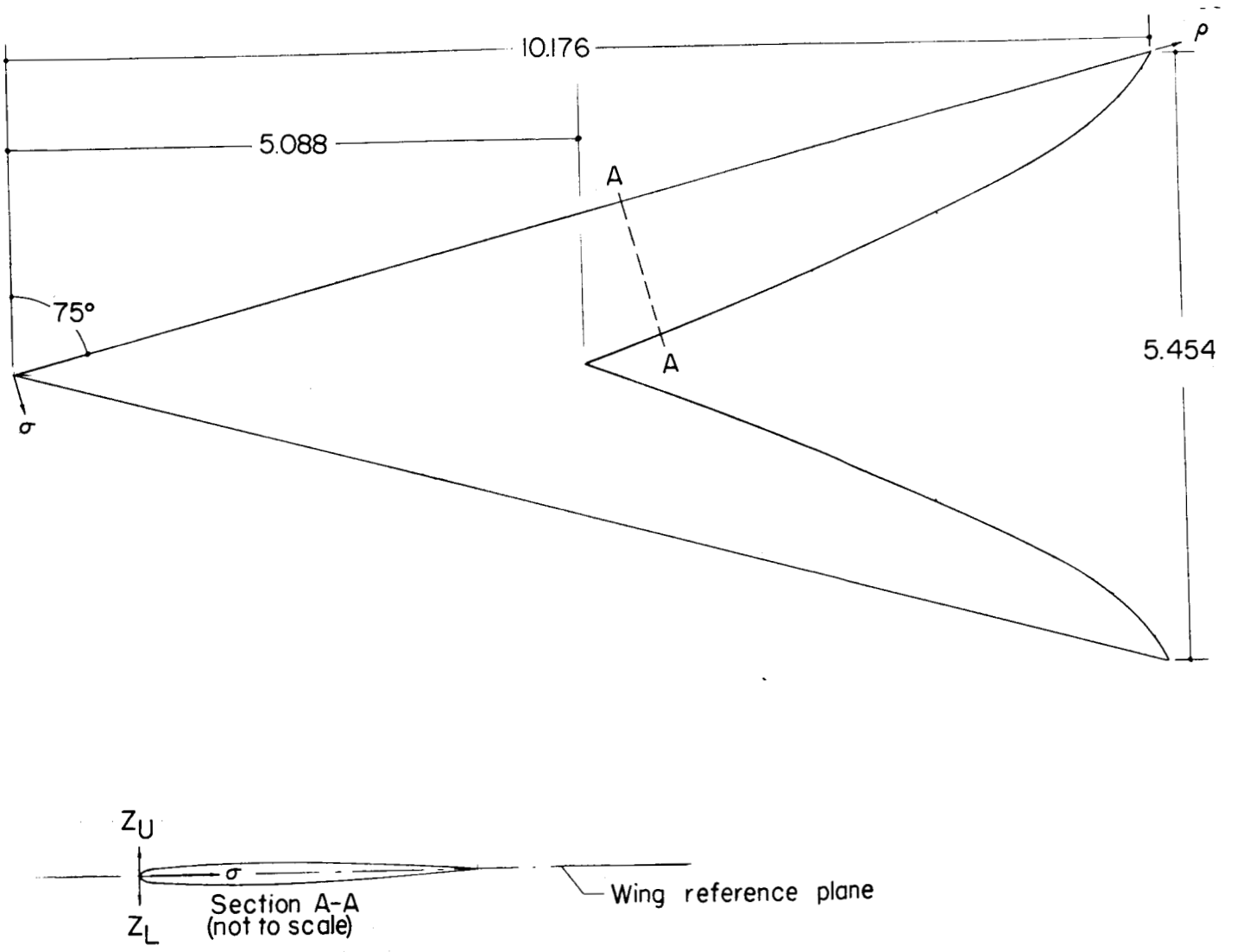

Figure 6.- Sketch of wing plan form (flat and twisted and cambered wings) showing nomenclature used in table I. Origin of ρ and σ at wing apex. (See table I for wing ordinates.)

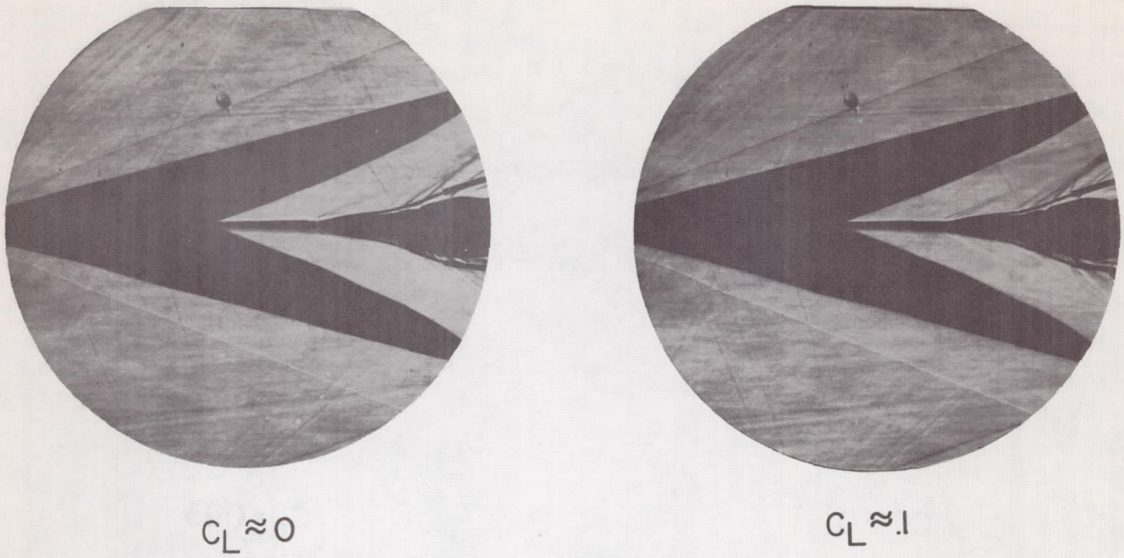

(a) Wing thickness I.

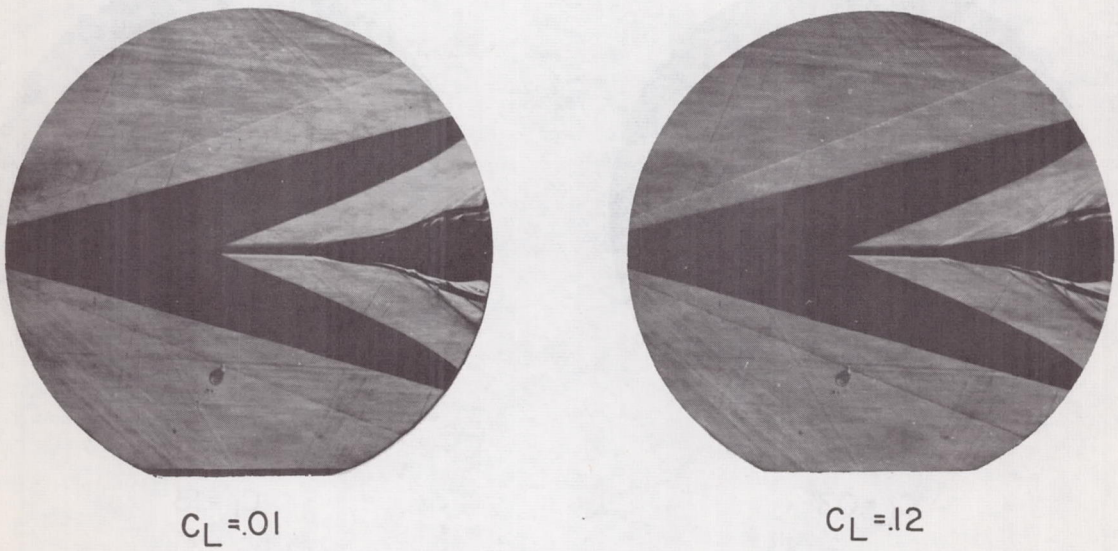

(b) Wing thickness II.

L-59-6031

Figure 7.- Typical schlieren photographs of the flat wings. Natural transition.

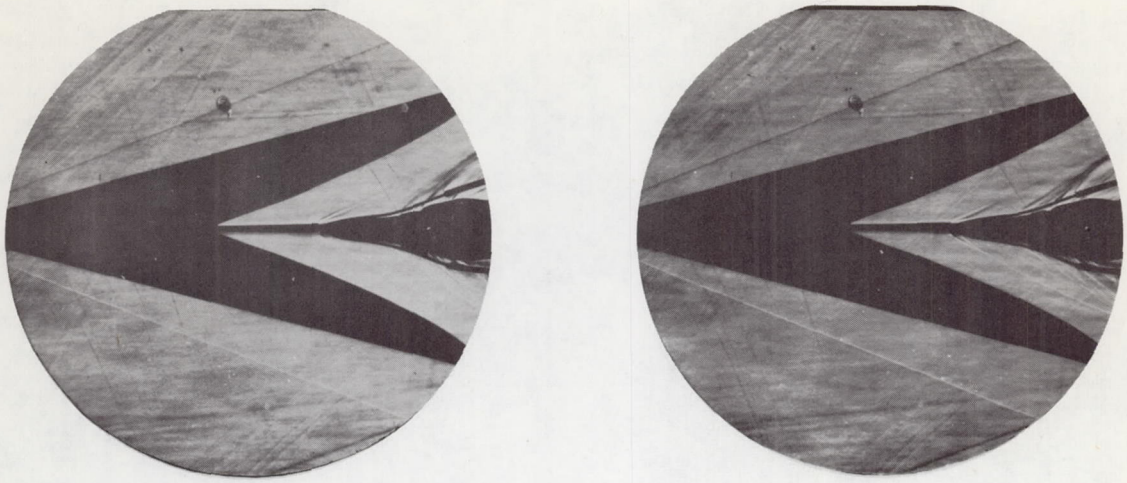

$C_L \approx 0$ $C_L = .093$

(a) Wing thickness I.

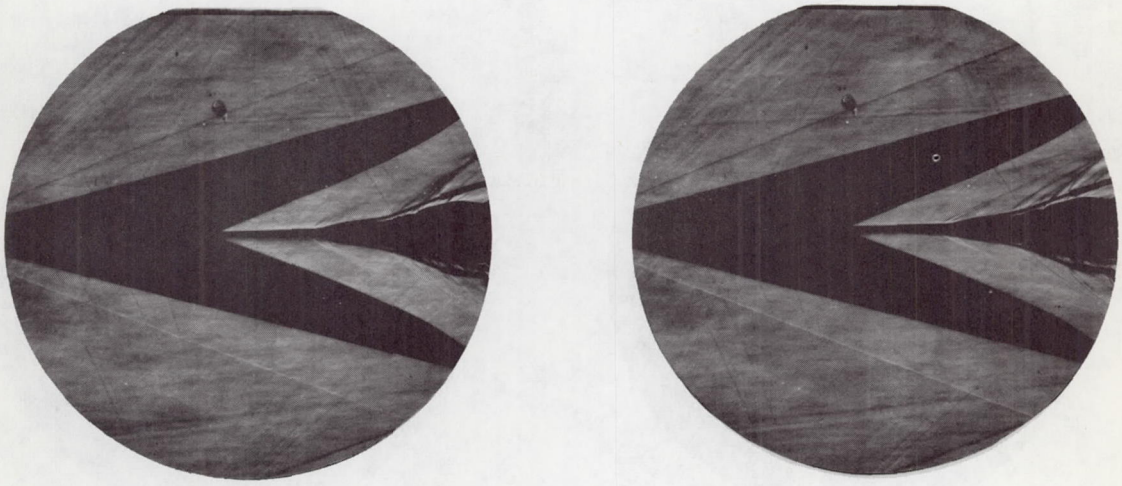

$C_L = .03$ $C_L = .13$

(b) Wing thickness II.

L-59-6032

Figure 8.- Typical schlieren photographs of the twisted and cambered wings. Natural transition.

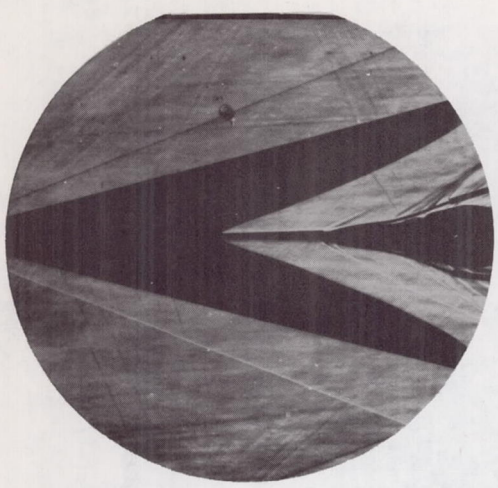

Natural transition, $C_L \approx .094$

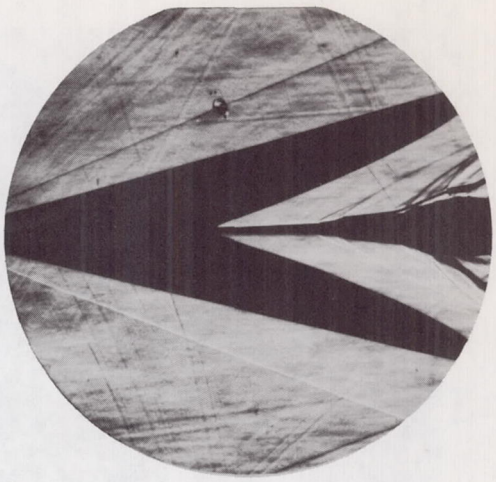

Fixed transition, $C_L \approx .092$

(a) Wing thickness I.

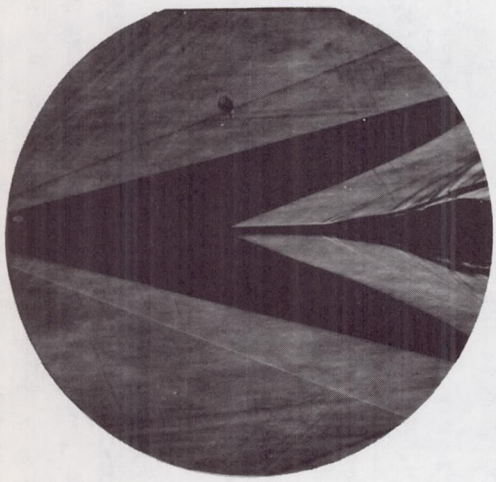

Natural transition, $C_L = .13$

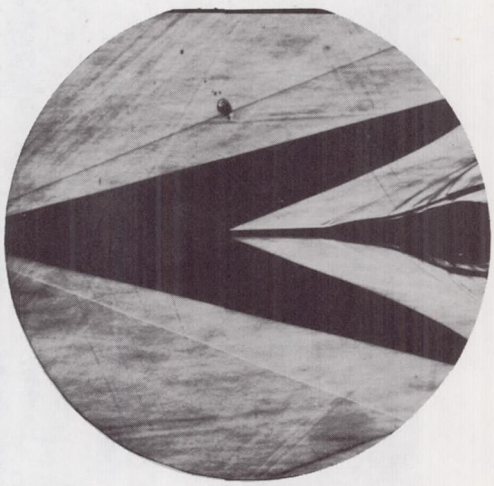

Fixed transition, $C_L = .12$

(b) Wing thickness II.

L-59-6033

Figure 9.- Schlieren photographs of the twisted and cambered wings at $C_L \approx 0.1$ for the natural- and fixed-transition cases.

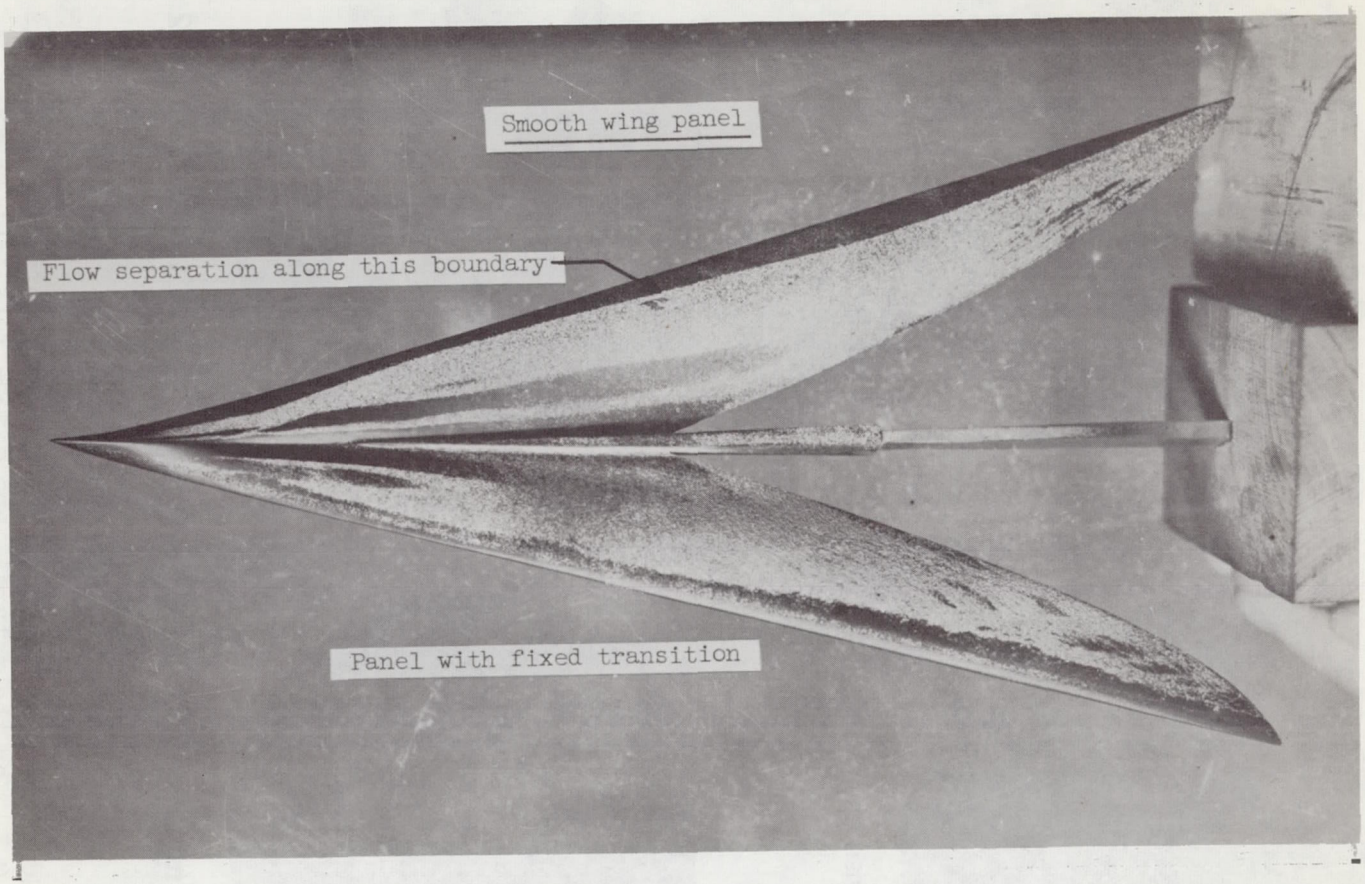

(a) Upper wing surface.

L-59-6034

Figure 10.- Liquid-film photograph of thick twisted and cambered wing. $C_L = 0.1$; $M = 2.91$; $R = 2.80 \times 10^6$. Transition strip, 0.005-0.008 inch high, 1/16 inch wide, 1/16 inch from wing leading edge; transition strip on one panel only.

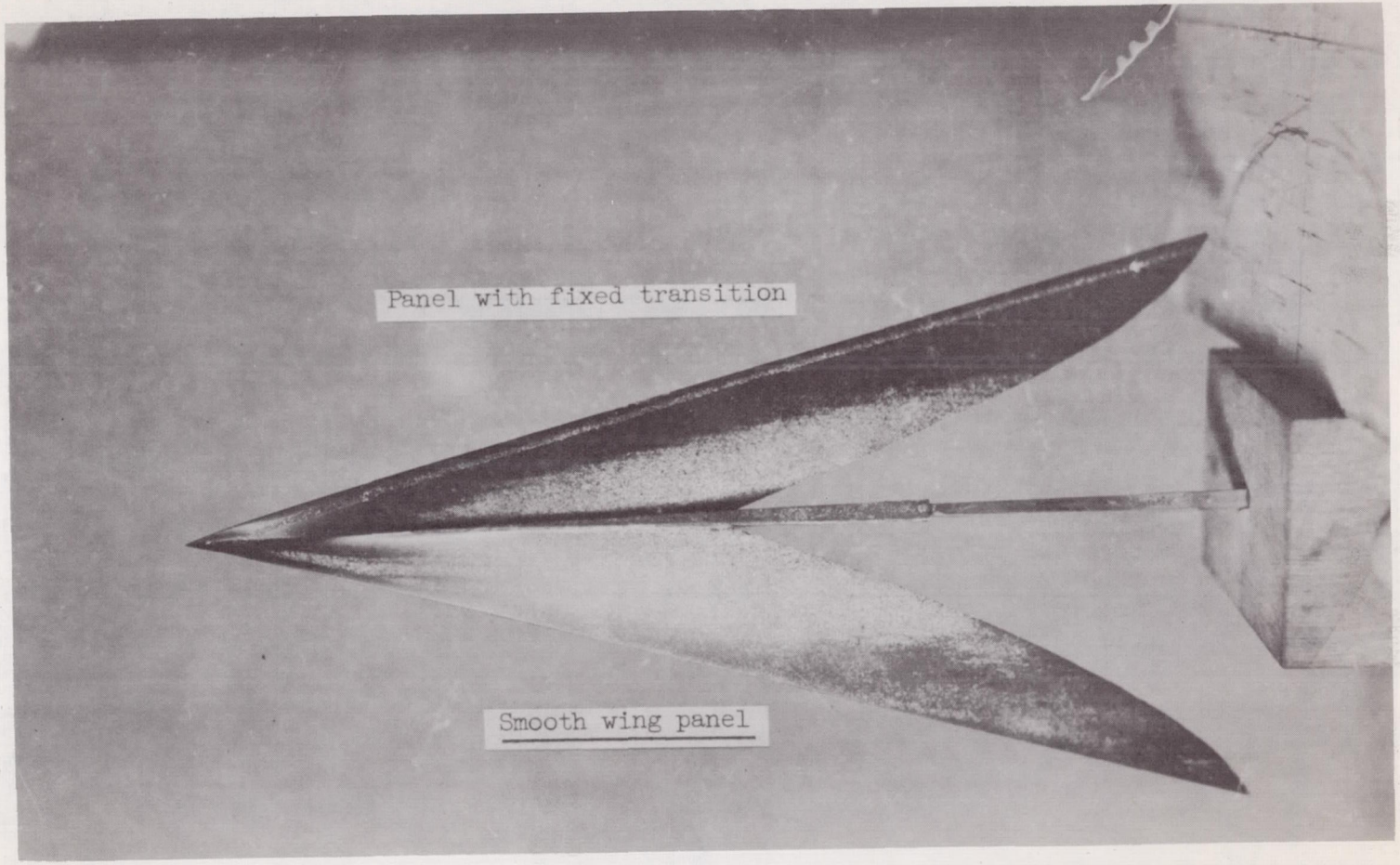

(b) Lower wing surface. L-59-6035

Figure 10.- Concluded.

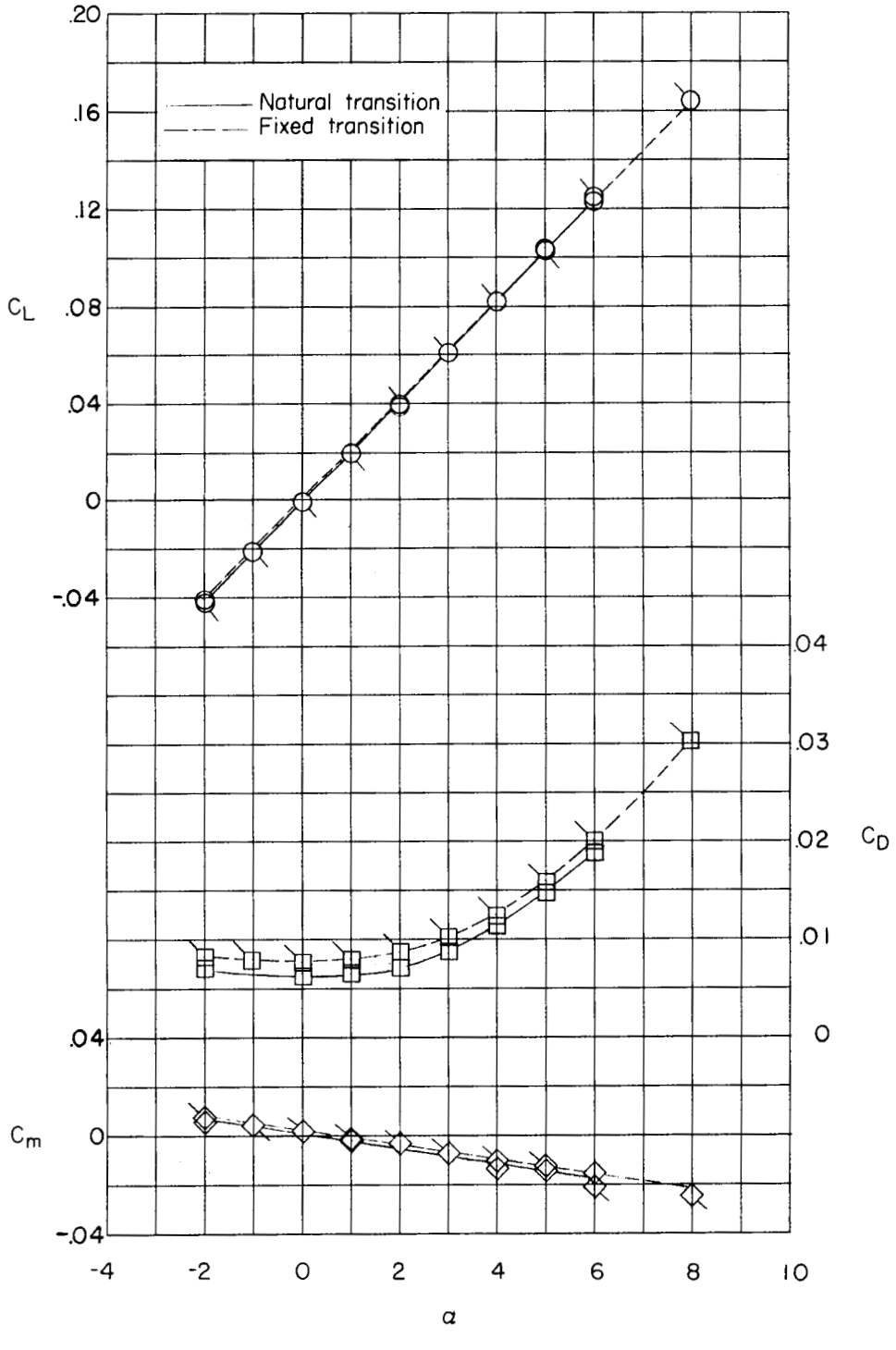

Figure 11.- Basic aerodynamic characteristics of the flat wing. Wing thickness I; flagged symbols denote fixed-transition data.

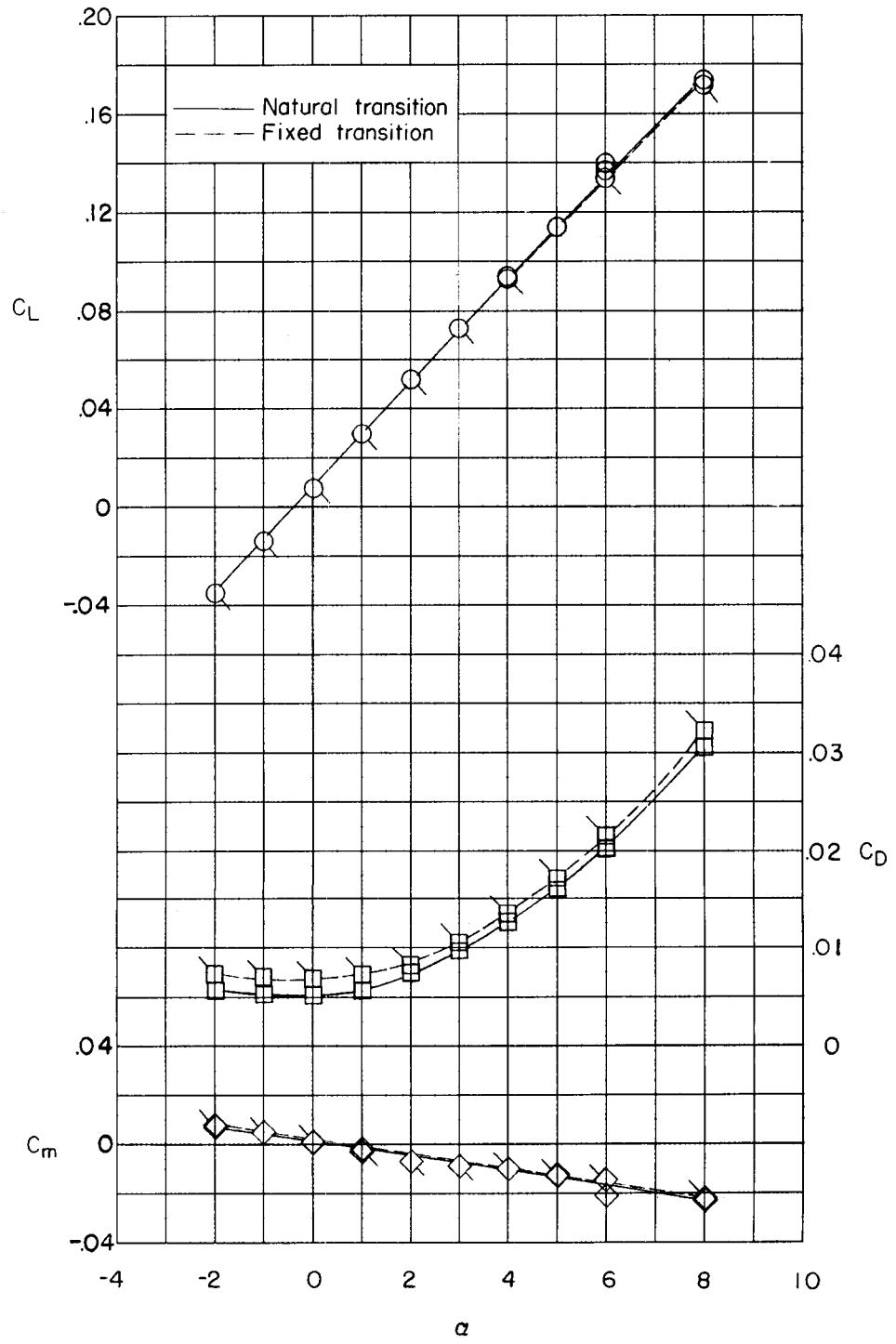

Figure 12.- Basic aerodynamic characteristics of the flat wing. Wing thickness II; flagged symbols denote fixed-transition data.

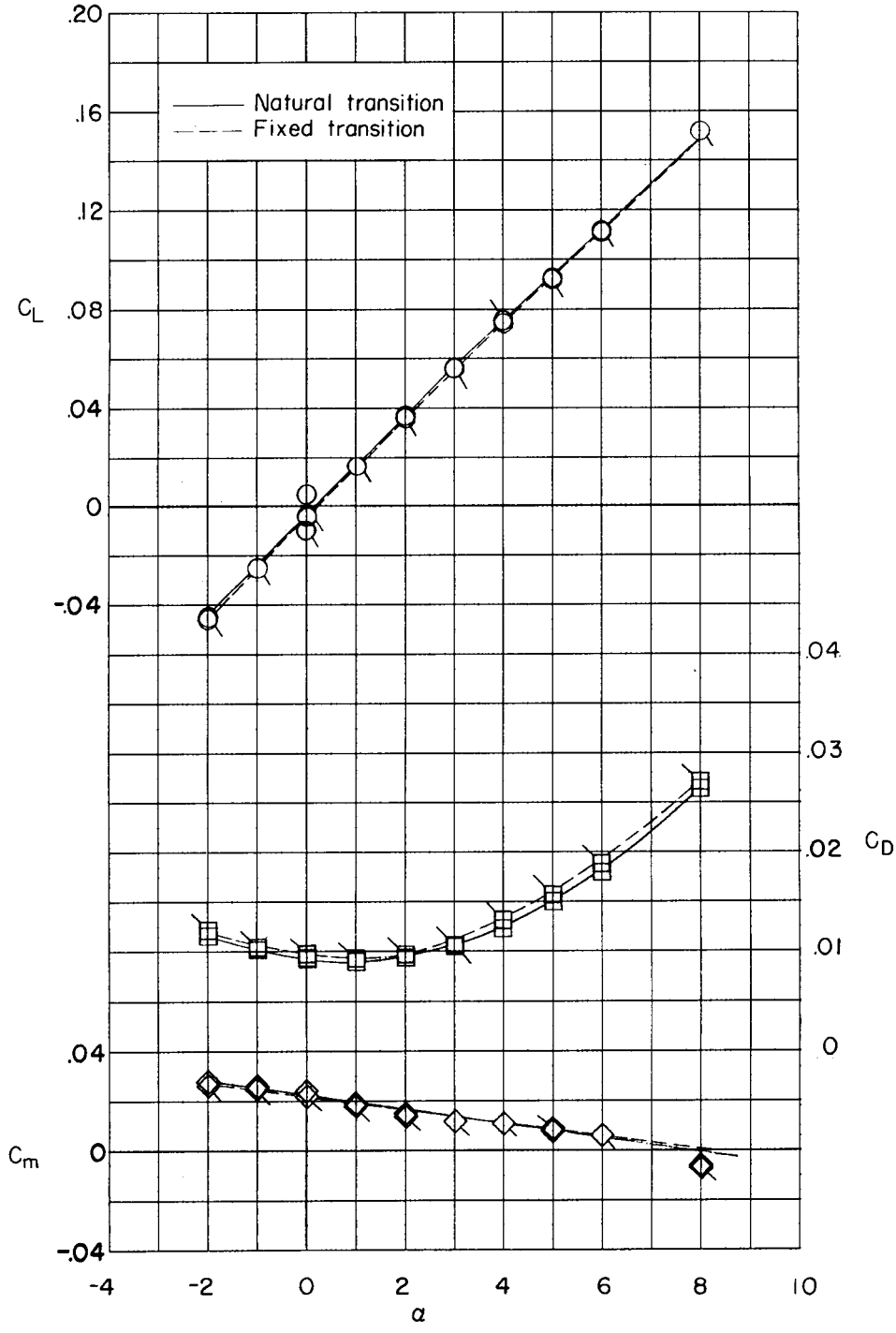

Figure 13.- Basic aerodynamic characteristics of twisted and cambered wing. Wing thickness I; flagged symbols denote fixed-transition data.

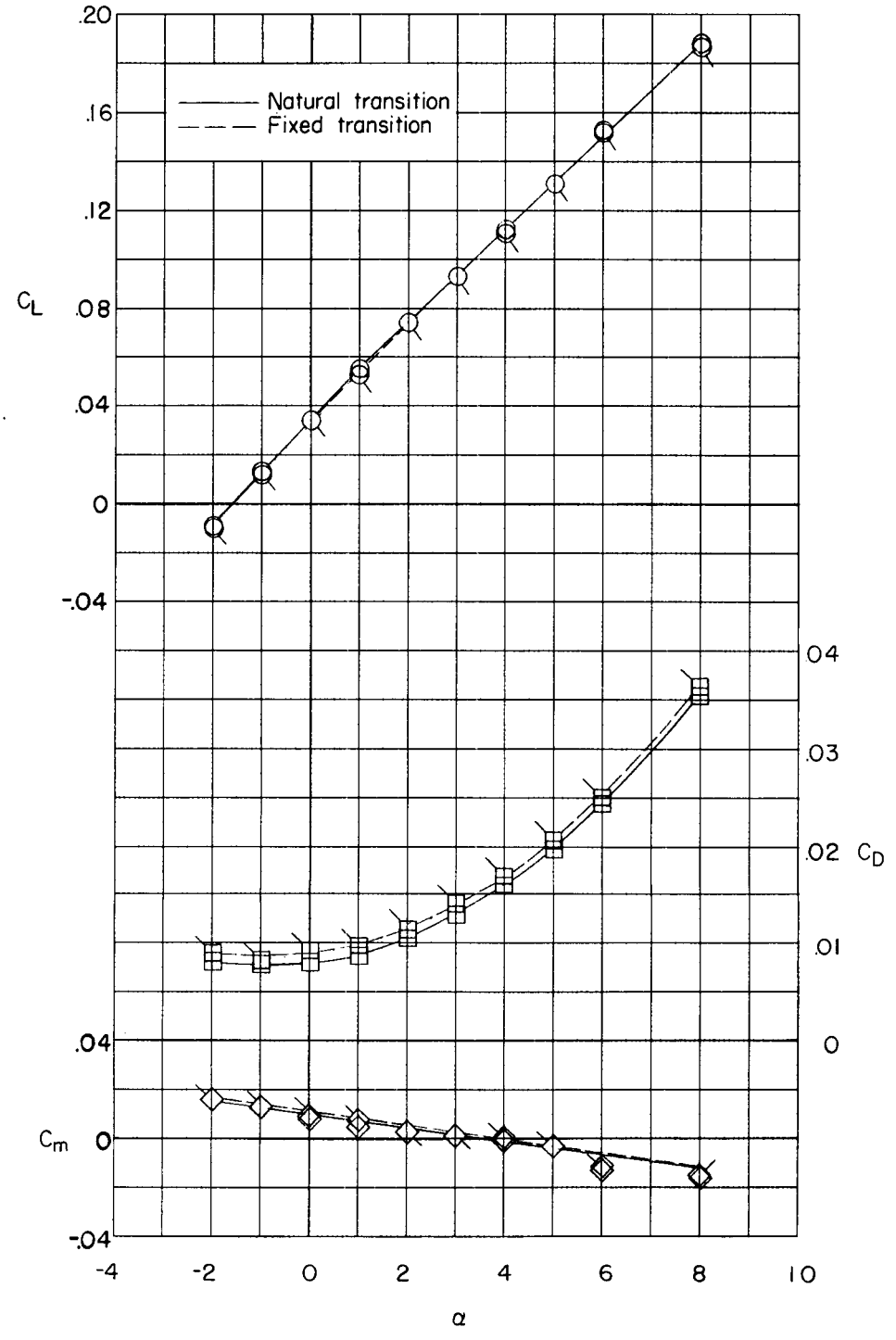

Figure 14.- Basic aerodynamic characteristics of the twisted and cambered wing. Wing thickness II; flagged symbols denote fixed-transition data.

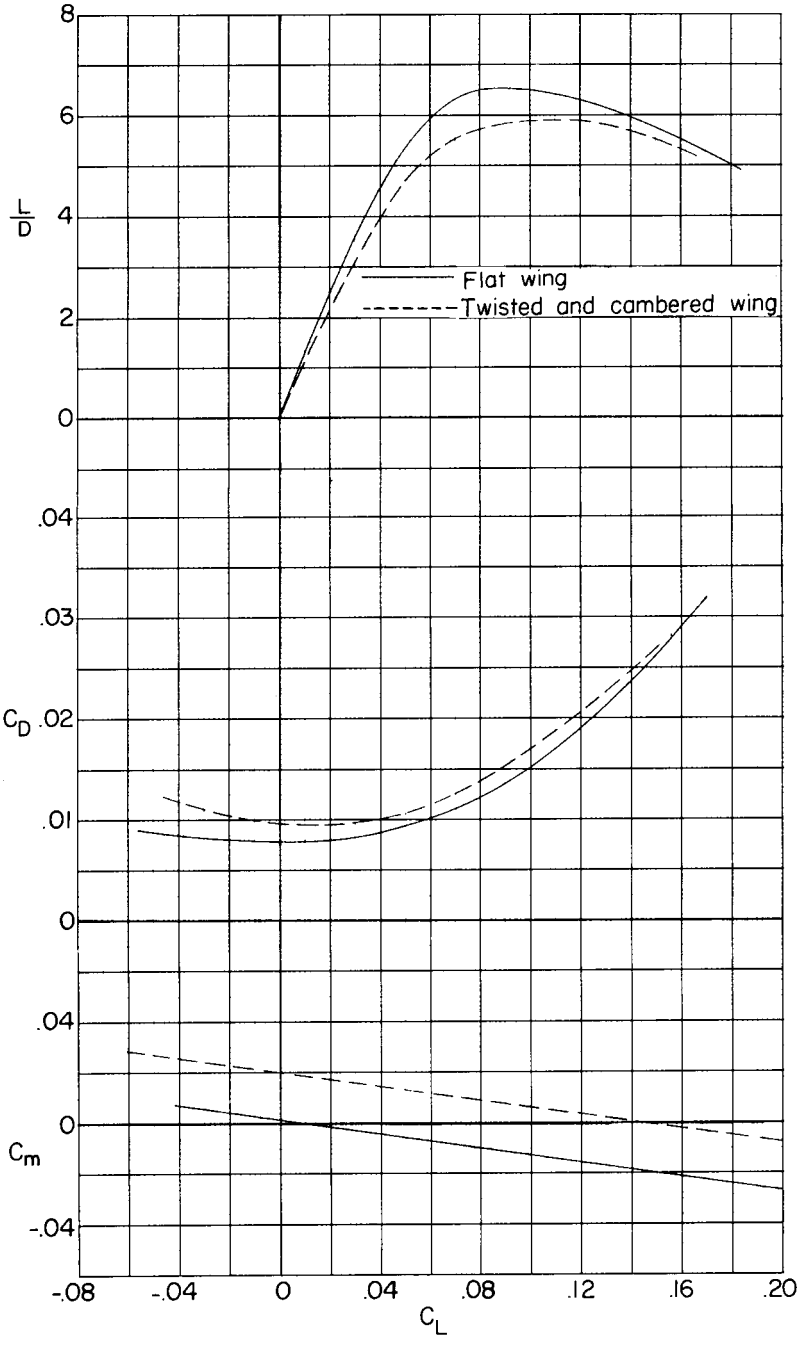

(a) Wing thickness I.

Figure 15.- Effect of twist and camber on wing aerodynamic characteristics. Fixed transition.

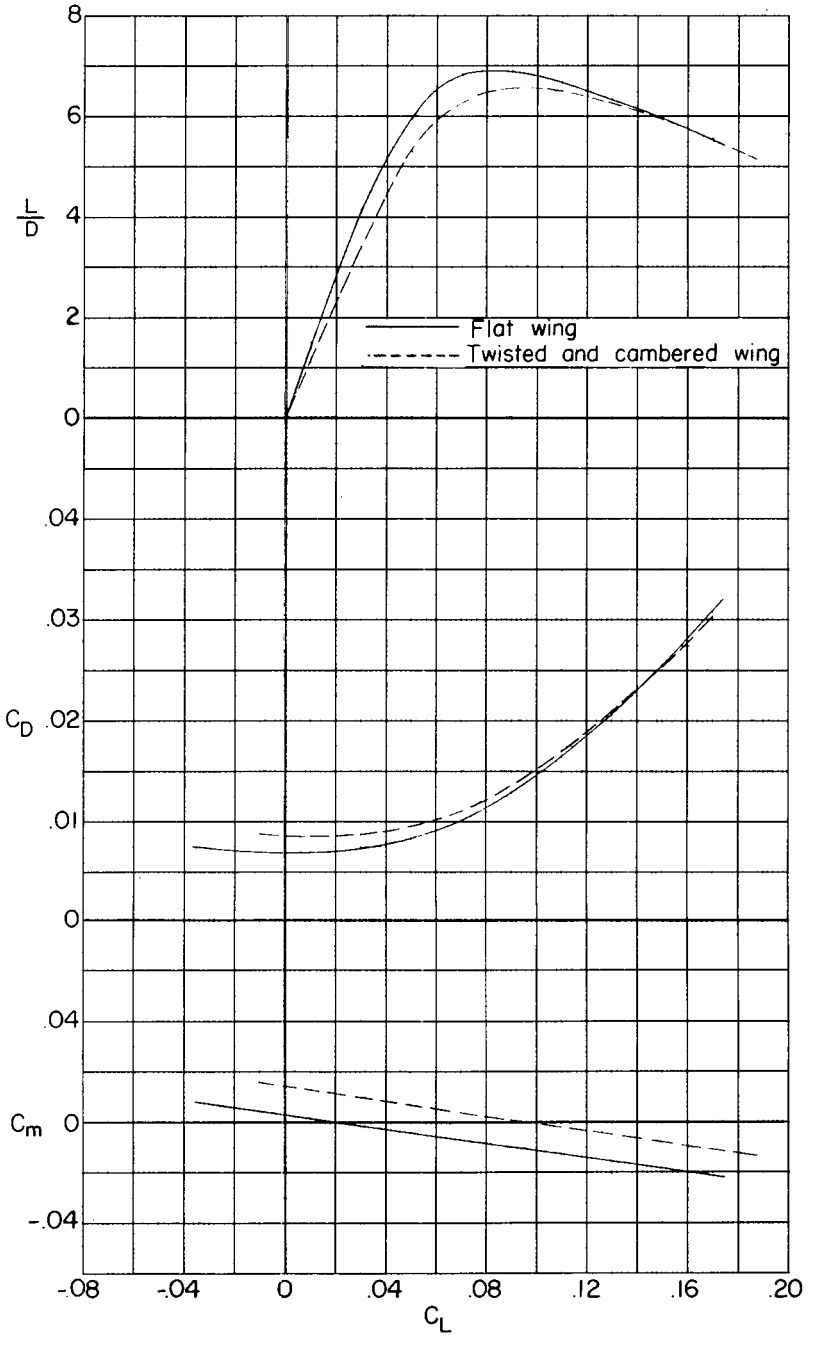

(b) Wing thickness II.

Figure 15.- Concluded.

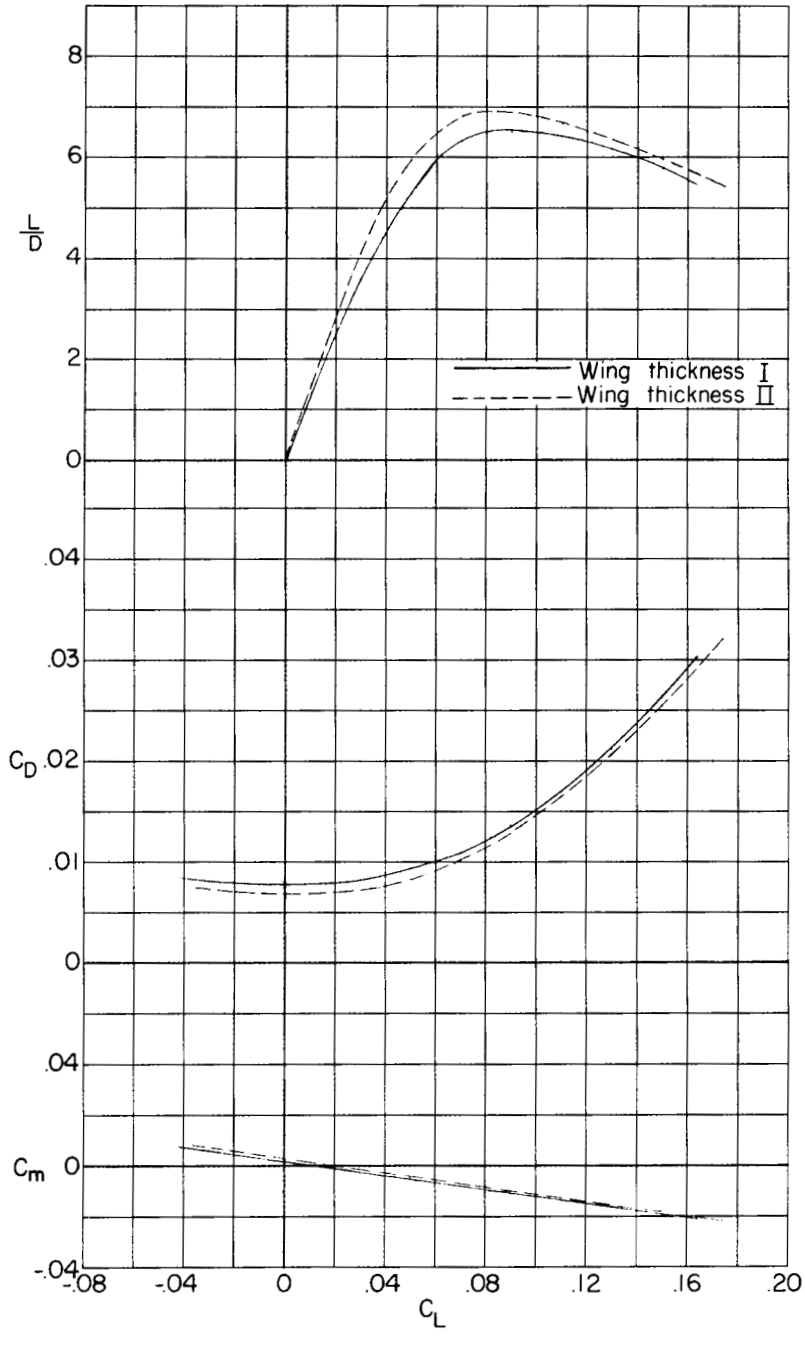

(a) Flat wings.

Figure 16.- Effect of thickness on the wing aerodynamic characteristics. Fixed transition.

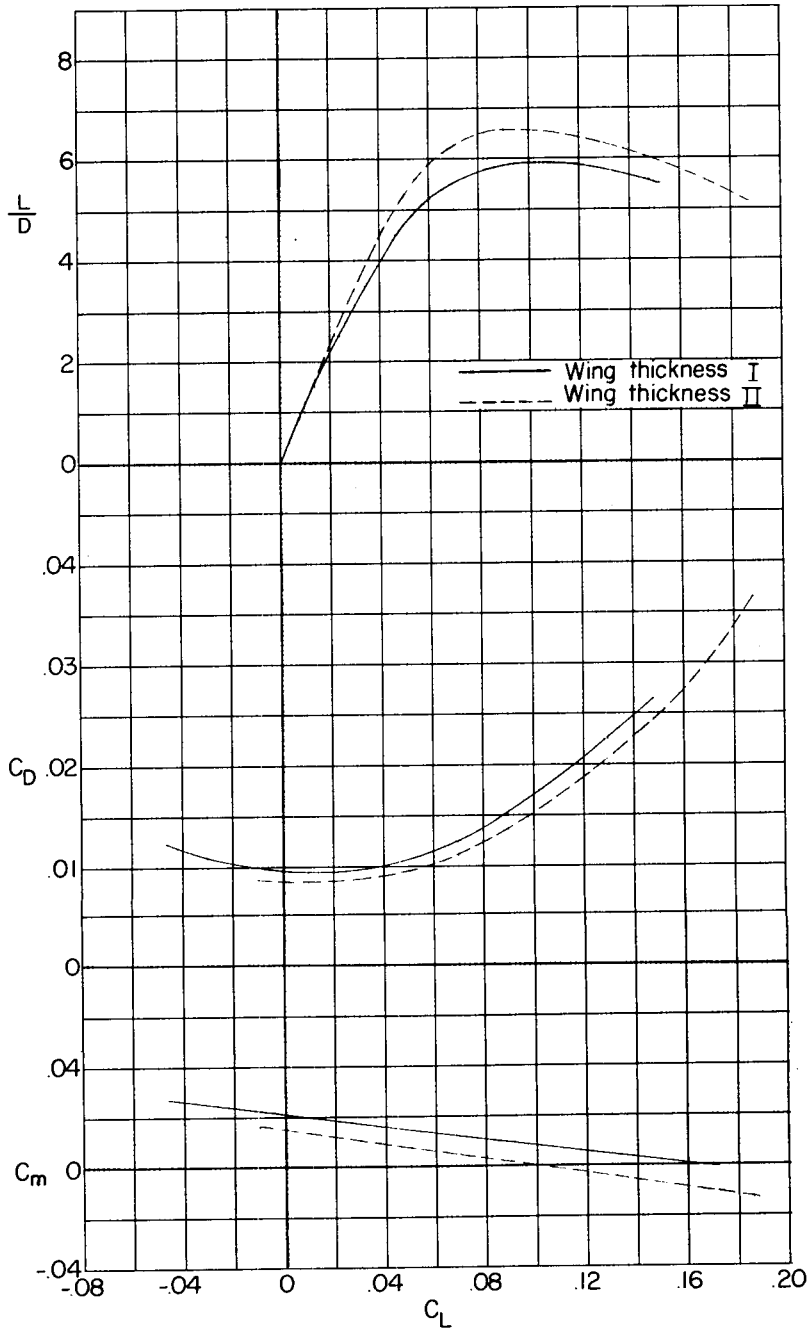

(b) Twisted and cambered wings.

Figure 16.- Concluded.

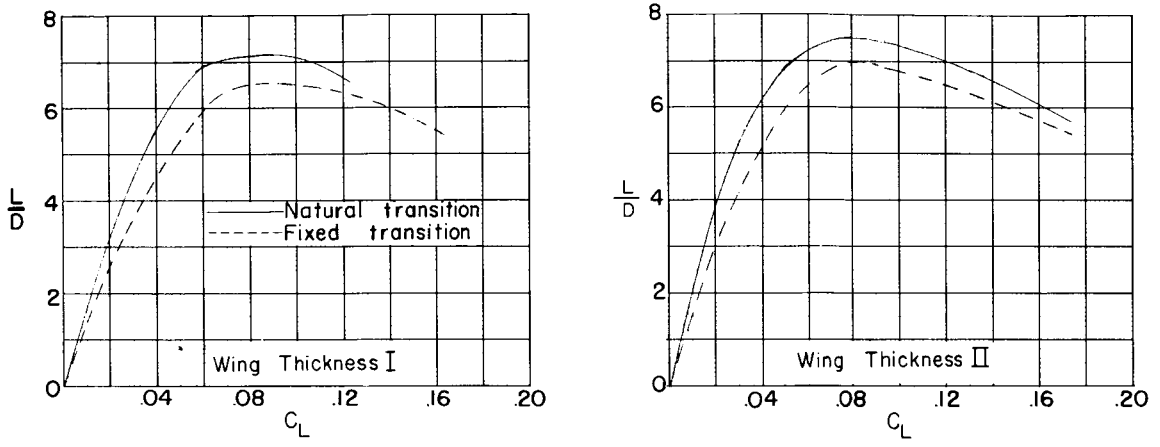

(a) Flat wings.

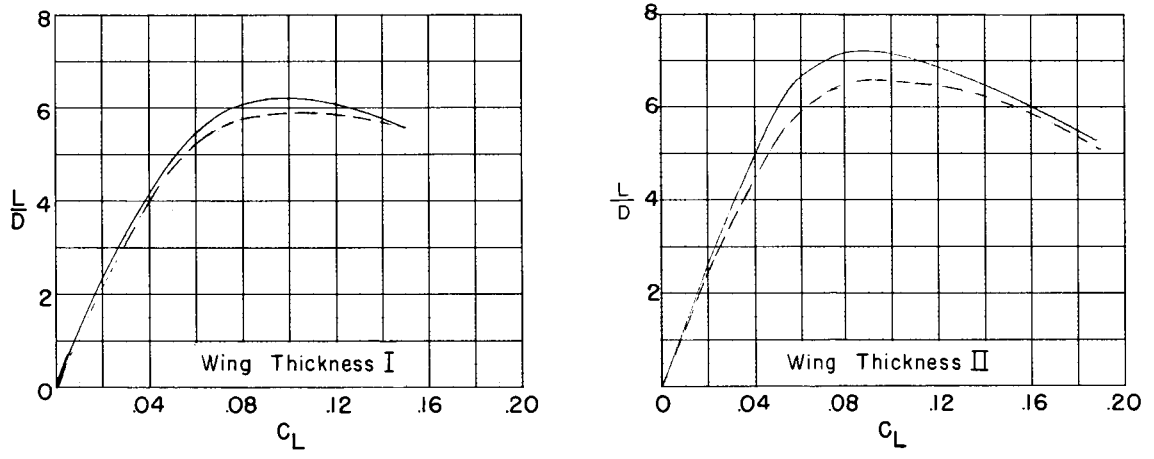

(b) Twisted and cambered wings.

Figure 17.- Summary of L/D characteristics of the flat and twisted and cambered wings.

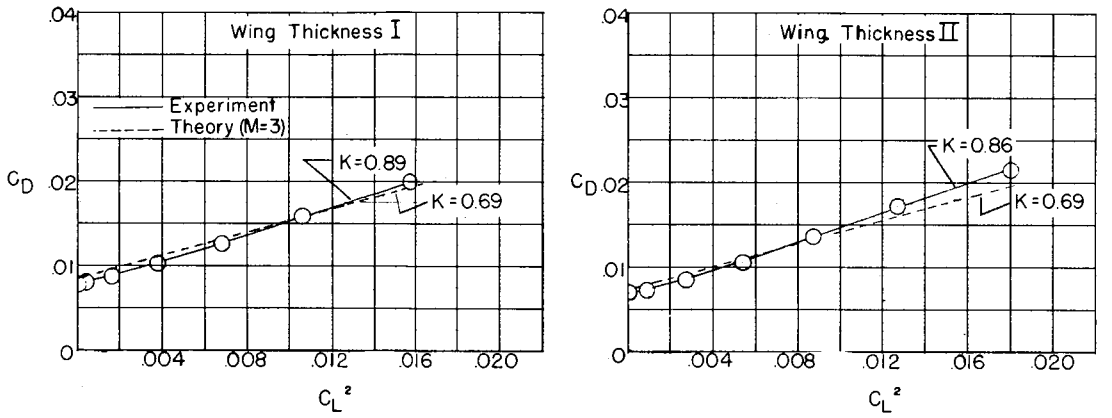

(a) Flat wings.

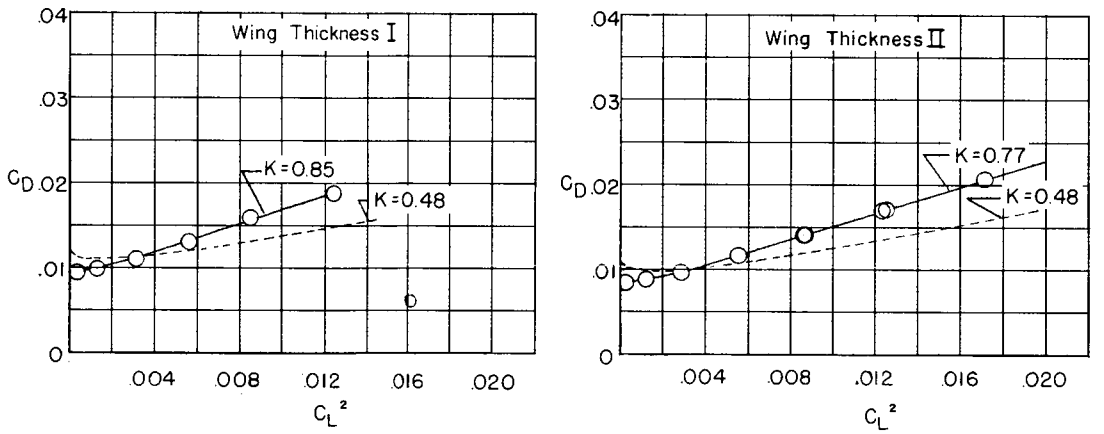

(b) Twisted and cambered wings.

Figure 18.- Drag-due-to-lift characteristics of the flat and twisted and cambered wings. Fixed transition.

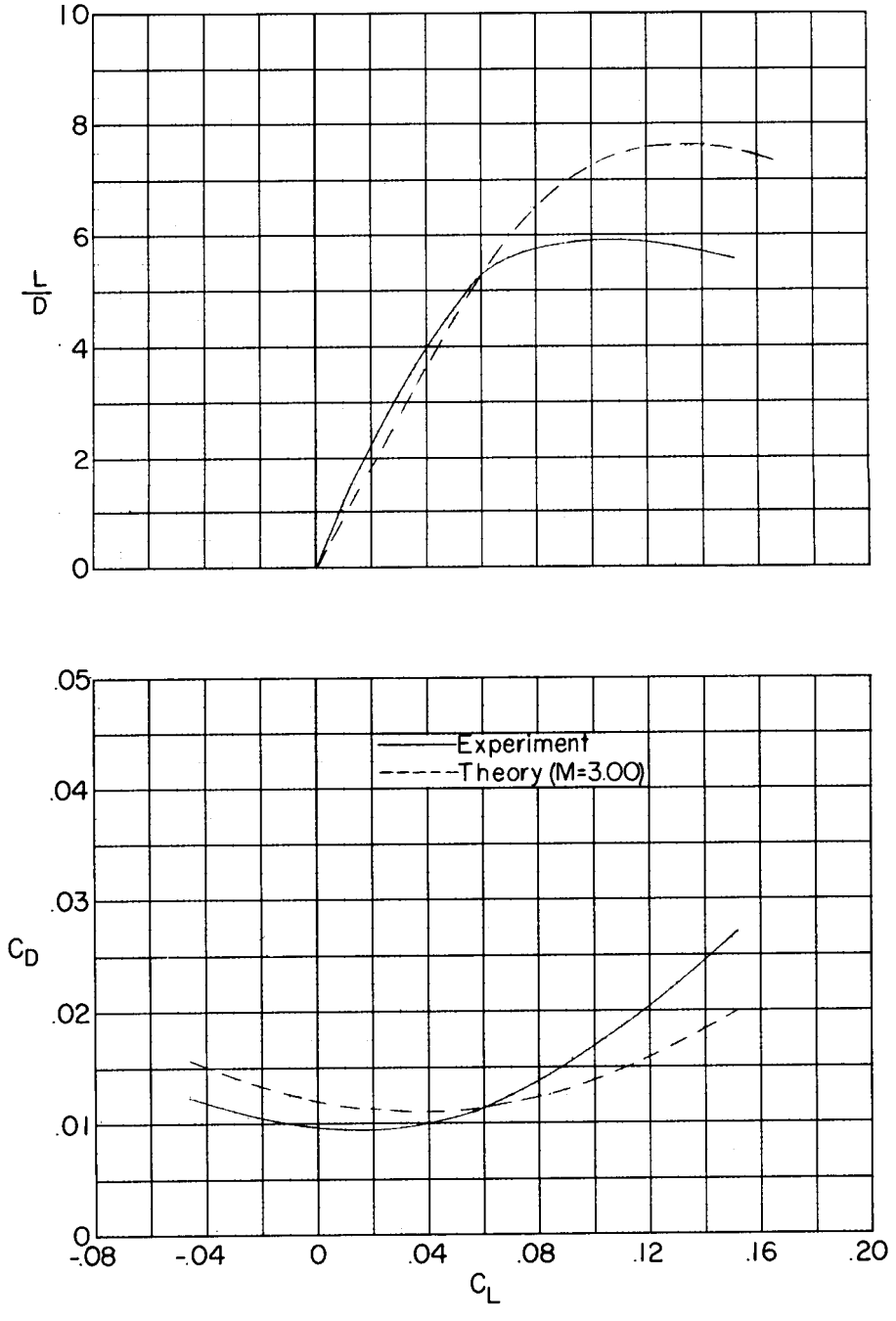

(a) Wing thickness I.

Figure 19.- Comparison of the theoretical and experimental characteristics of the twisted and cambered wings. Fixed transition.

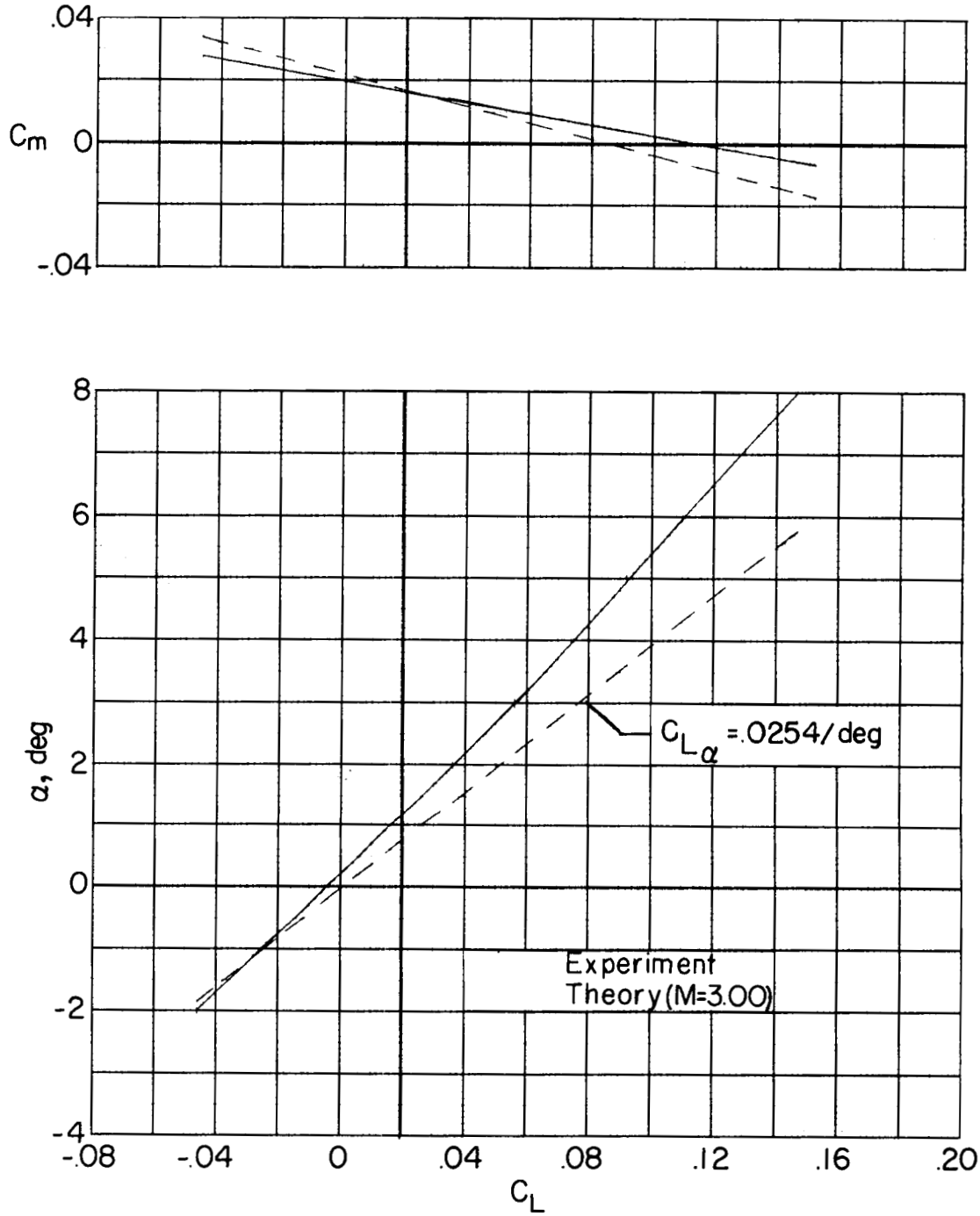

(a) Concluded.

Figure 19.- Continued.

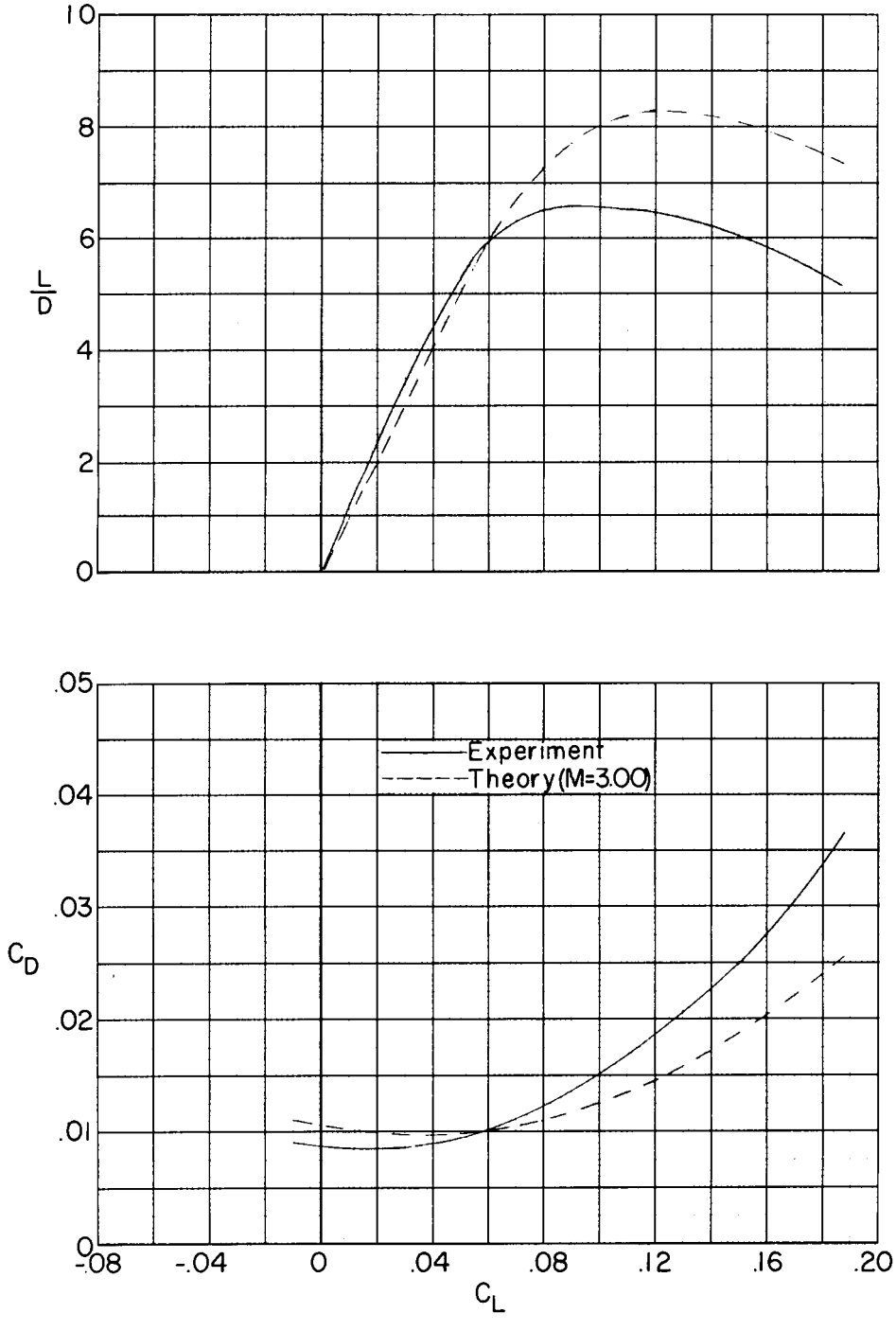

(b) Wing thickness II.

Figure 19.- Continued.

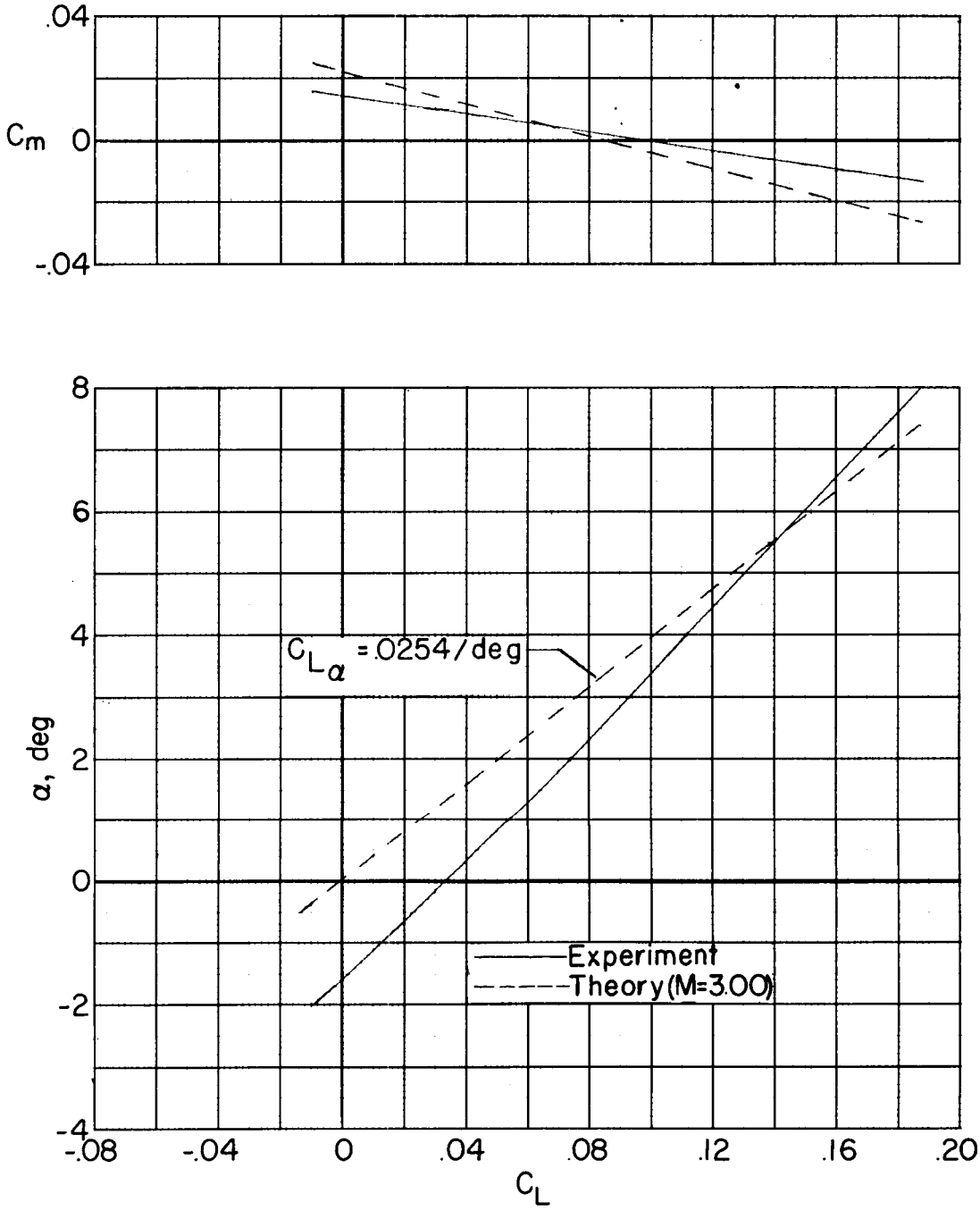

(b) Concluded.

Figure 19.- Concluded.

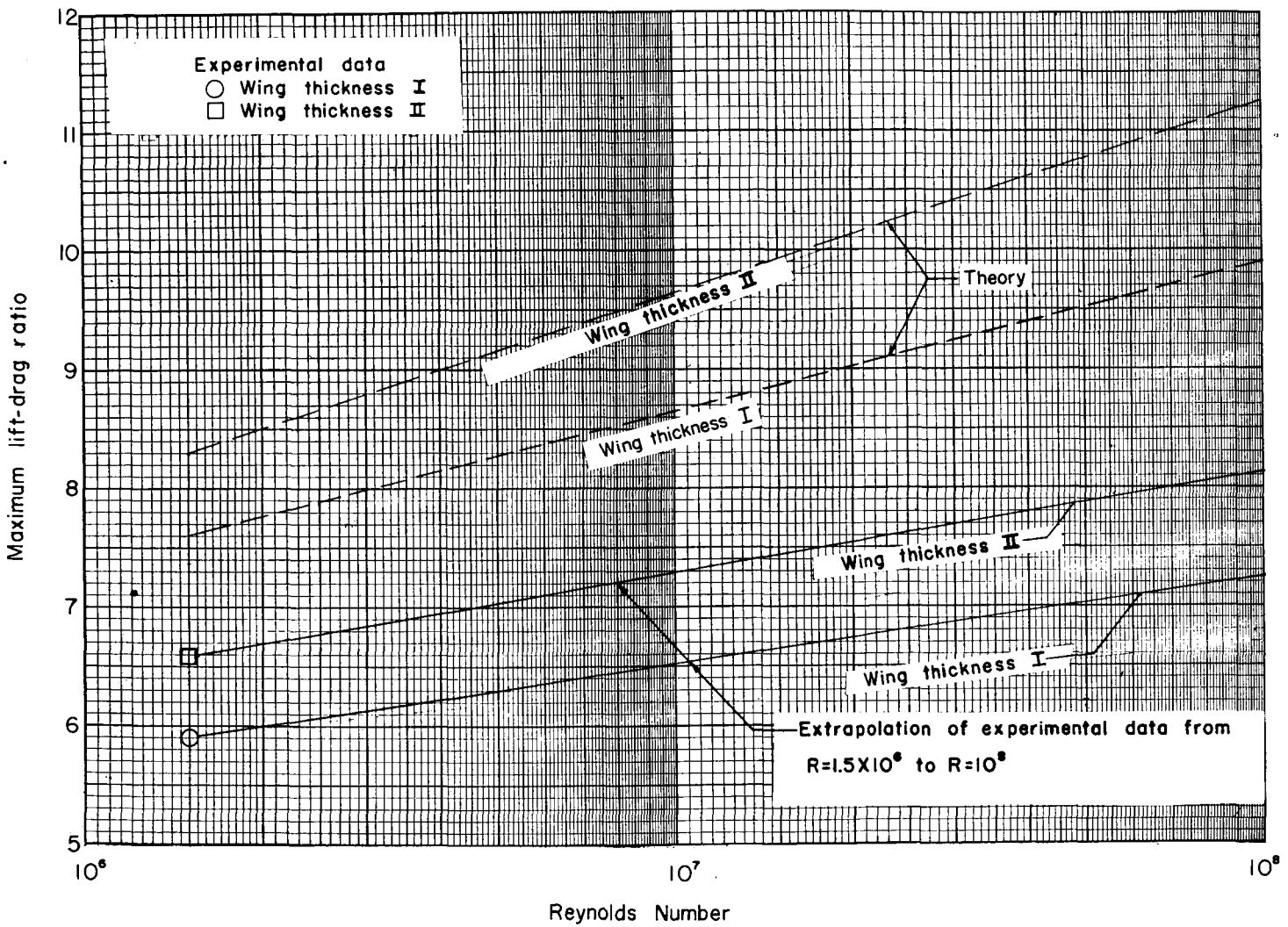

Figure 20.- Extrapolated $(L/D)_{max}$ values of the twisted and cambered wings. Turbulent boundary layer.

Symbols	R×10⁻⁶	Transition Strip l, in.	Transition Strip w, in.	$C_{D,min}$	(Grit size, in.)² × 10⁴
○	0.78	None	None	0.0065	0
○	0.78	None	None	0.0069	0
□	2.80	None	None	0.0064	0
◇	1.50	None	None	0.0064	0
△	0.78	1/4	1/8	0.0069	0.062
△	0.78	1/4	1/8	0.0079	0.160
△	0.78	1/4	1/8	0.0075	0.422
△	0.78	1/4	1/8	0.0078	0.422
▽	0.78	1/4	1/16	0.0070	0.160
▷	0.78	1/16	1/16	0.0072	0.422
◁	0.78	1/16	1/32	0.0070	0.422
◸	1.50	3/32	1/16	0.0078	0.422
◹	2.80	1/16	1/32	0.0076	0.422
◺	2.80	1/16	1/16	0.0078	0.422
◿	2.80	1/4	1/8	0.0074	0.422

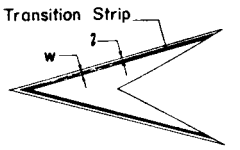

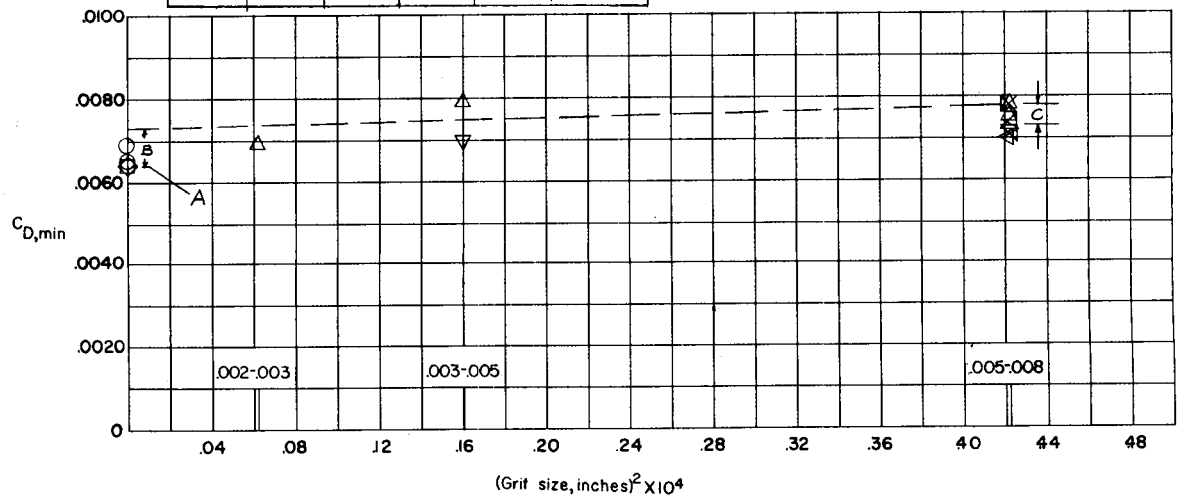

(a) Flat (thick) wing.

Figure 21.- Effect of roughness grain size on the wing drag.

Symbols	R×10⁻⁶	Transition Strip l, in.	Transition Strip w, in.	$C_{D,min}$	(Grit size, in.)² x 10⁴
○	0.78	None	None	0.0057	0
◇	1.50	None	None	0.0050	0
◇	1.50	None	None	0.0052	0
◸	1.50	3/32	1/16	0.0066	0.160
◸	1.50	3/32	1/16	0.0069	0.422
▱	2.35	None	None	0.0056	0
▱	2.35	3/32	1/16	0.0064	0.160
▱	2.35	3/32	1/16	0.0068	0.160
◺	1.50	3/32	1/16	0.0060	0.160
◿	0.40	3/32	1/16	0.0057	0.160

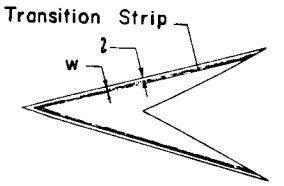

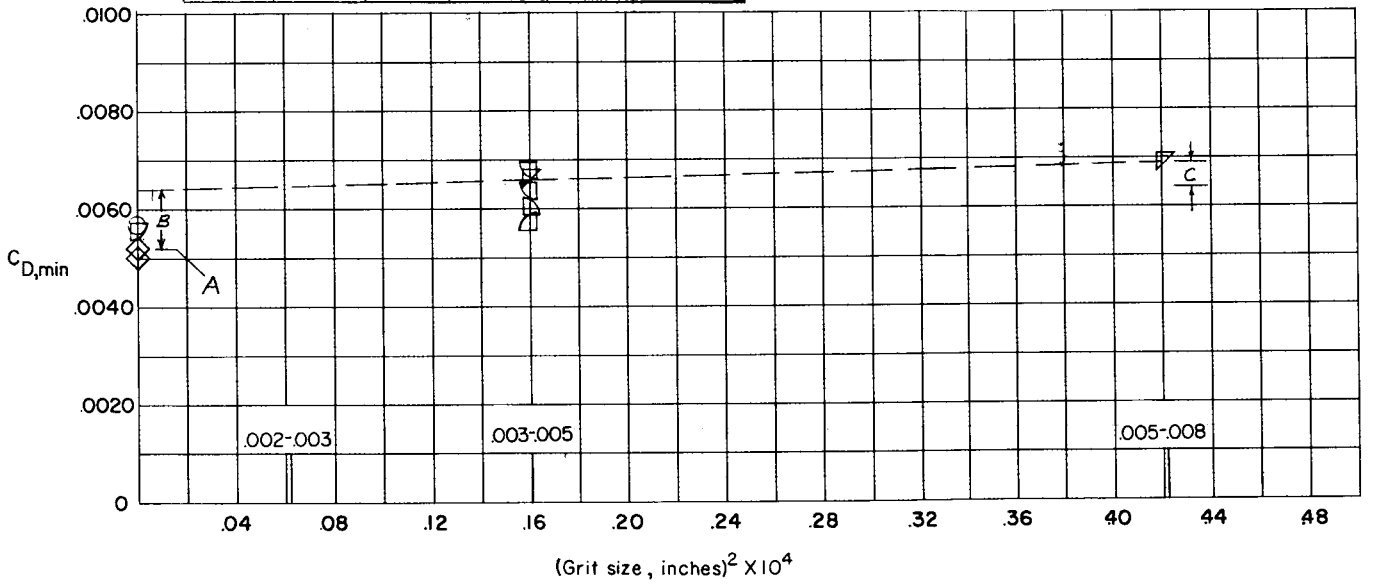

(b) Flat (thin) wing.

Figure 21.- Continued.

Symbols	$R \times 10^{-6}$	Transition Strip		$C_{D,min}$	$(\text{Grit size, in.})^2 \times 10^4$
		l, in.	w, in.		
○	0.78	None	None	0.0078	0
□	2.80	None	None	0.0087	0
◇	1.50	None	None	0.0087	0
	1.50	None	None	0.0090	0
▷	0.78	1/16	1/16	0.0099	0.160
▽	1.50	3/32	1/16	0.0094	0.422
△	2.80	1/16	1/16	0.0100	0.422

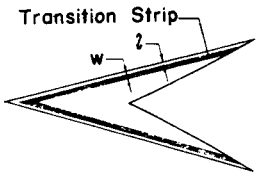

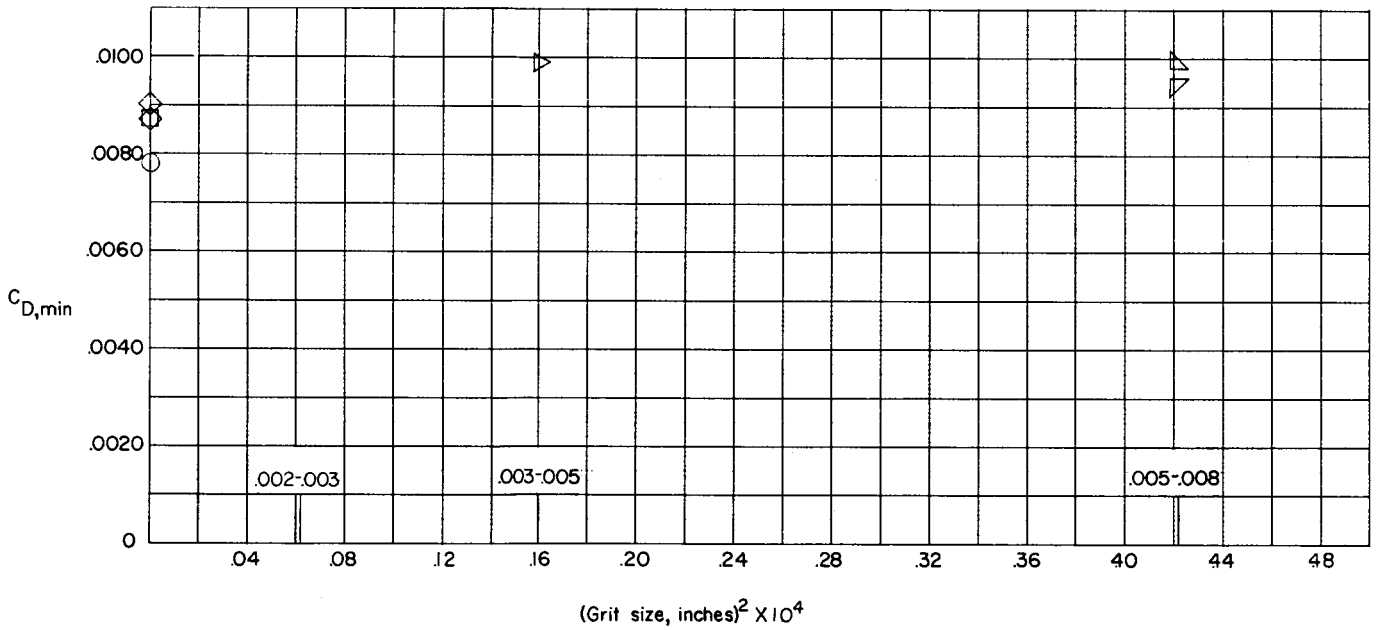

(c) Twisted and cambered (thick) wing.

Figure 21.- Continued.

Symbols	R×10^{-6}	Transition Strip		$C_{D,min}$	(Grit size, in.)^2 x 10^4
		l, in.	w, in.		
◇	1.50	None	None	0.0078	0
◸	1.50	3/32	1/16	0.0085	0.422
⏍	1.50	1/16	1/16	0.0090	0.422
⏏	2.50	1/16	1/16	0.0089	0.422

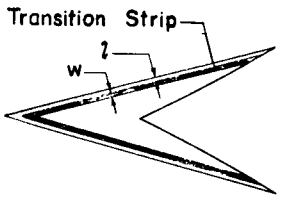

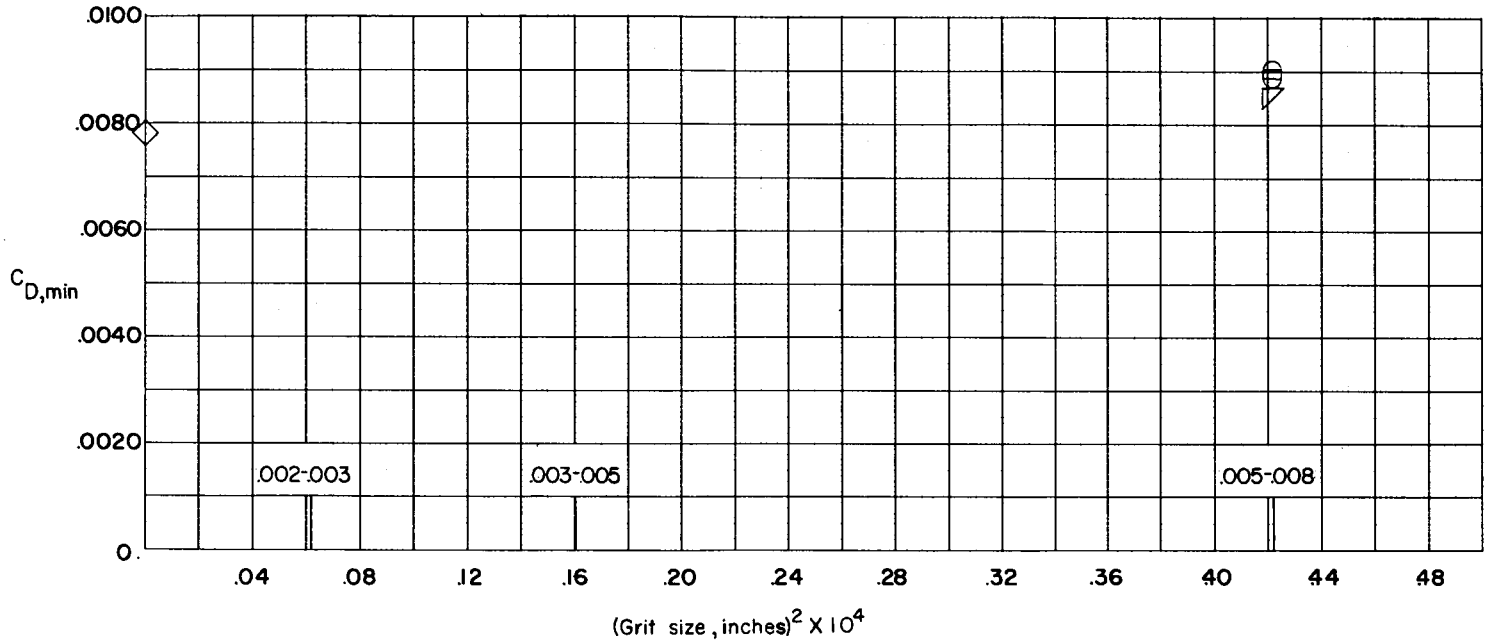

(d) Twisted and cambered (thin) wing.

Figure 21.- Concluded.

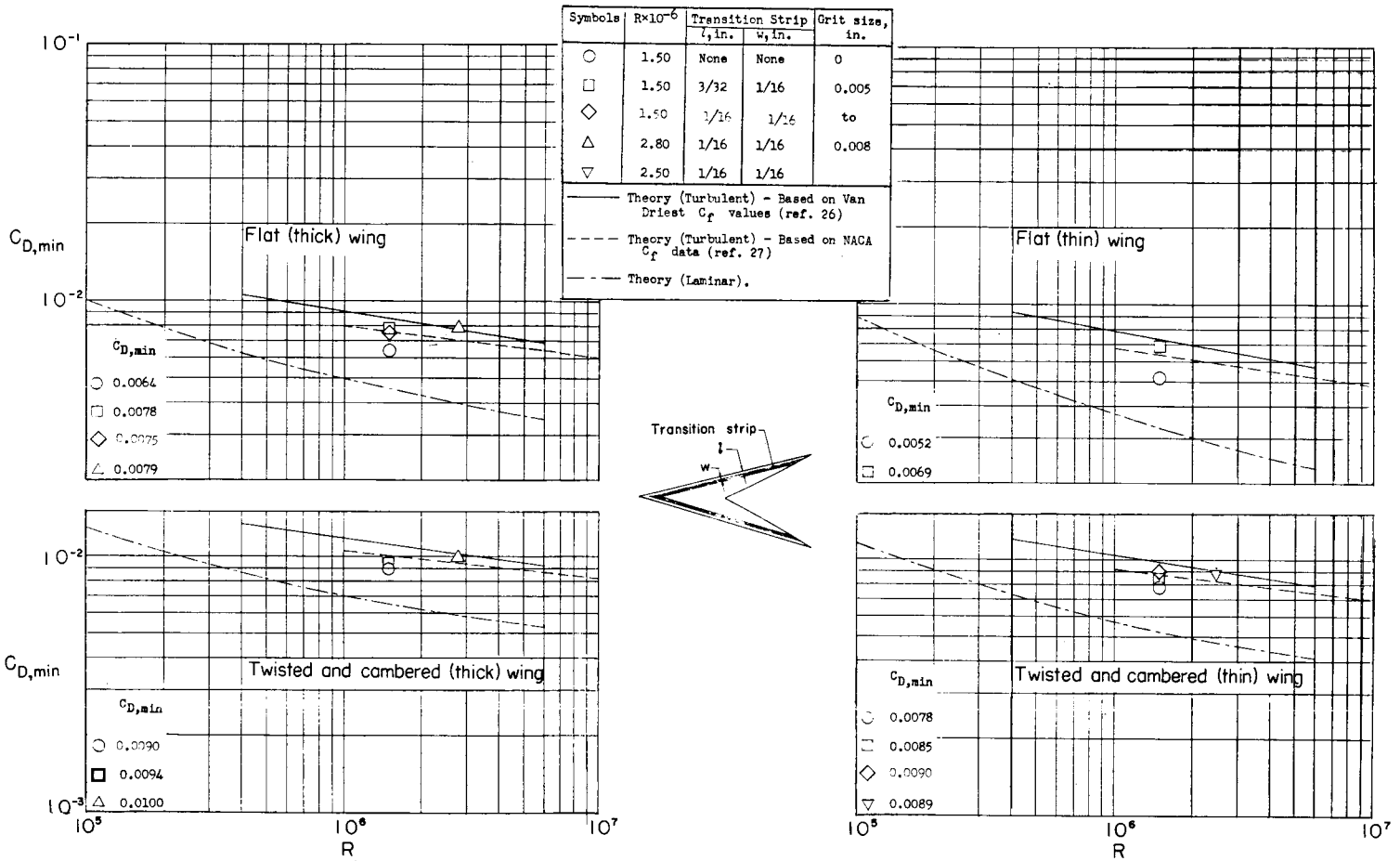

Figure 22.- Variation of $C_{D,min}$ with Reynolds numbers for the wings with and without transition strips.